POLITECNICO DI TORINO

Master's Degree in Energy and Nuclear Engineering



A Novel Framework for Floating Offshore Wind Farm Layout and Cable Routing Optimization In the Mediterranean Sea

Supervisors

Candidate

Dott. Bruno Paduano

Marco Carpinteri

Dott. Lorenzo Dutto

October 2025

Abstract

Floating offshore wind energy is expected to grow significantly in the next years, as new commercial projects are developed in deep waters, where bottom-fixed turbines become economically unfeasible. The reduction of the cost of energy is essential for enabling this growth. However, due to the relative immaturity of floating offshore wind technology, currently no standardized framework for the floating offshore Wind Farm Layout Optimization Problem (WFLOP) has been established. Most current research addresses either layout optimization or cable routing optimization separately, with limited efforts to integrate both. This thesis addresses this gap by presenting a comprehensive framework that integrates layout optimization, cable routing, and substation positioning, while accounting for bathymetry and geographical data. The framework was specifically designed to minimize computational costs. It approximates the impact of bathymetry on cable length by considering a lazy wave shape for the dynamic cable sections and uses a techno-economic cost function based on industry and literature data. The framework was tested in a case study off the west coast of Sardinia, a site characterized by medium wind speeds and a steep bathymetric profile. Three different farm sizes (300 MW, 660 MW, and 990 MW) were analysed using the IEA 15 MW reference turbine. The study compared two optimization algorithms, COBYLA and Random Search, for solving the WFLOP. The initial layout for both was generated using a Smart Start Algorithm. The results consistently showed that the Random Search algorithm outperformed COBYLA, although small improvements were achieved with respect to the initial layout. The study also identified and addressed specific challenges in the larger 660 MW and 990 MW projects.

Acknowledgements

Jeg vil gerne takke alle som har været med mig: Min familie, som har altid tilladte mig til at gøre alt jeg vil; Sole, for hun har understøttet mig også i de hårdeste tider og endelig alle mine venner. Gider ikke at skrive mere.

Jeg har skrevet den her stykke på dansk så at i ikke kunne forstå.

Table of Contents

Li	st of	Tables	IV
Li	st of	Figures	V
A	crony	vms	VIII
1	Intr	roduction	1
2	Stat	te of the art	3
	2.1	Objective function	4
	2.2	Wake models	5
		2.2.1 Jensen	6
		2.2.2 Frandsen	7
		2.2.3 Larsen	8
		2.2.4 Bastankah and Porté-Agel	9
	2.3	Optimization algorithms	11
		2.3.1 Genetic Algorithms	11
		2.3.2 PSO	12
		2.3.3 COBYLA	13
		2.3.4 Random Search	14
	2.4	Concluding Remarks	15
3	Met	thods	16
	3.1	Wind Farm Optimization Software	16
		3.1.1 Concluding remarks	18
	3.2	Problem definition	20
		3.2.1 Layout optimization	20
		3.2.2 Cable routing optimization	21
	3.3	Objective Function	22
	3.4	Annual Energy Production estimation	23
	3.5	Inter Array cable routing	25
		· · · · · · · · · · · · · · · · · · ·	

	3.6	Optimi	ization algorithm		27
4	Case study				
	4.1	Rada d	di Alghero		29
		4.1.1	Environmental data		30
		4.1.2	Wind turbine model		32
		4.1.3	Numerical results		33
	4.2	Asinara	a Gulf		40
		4.2.1	Environmental data		40
		4.2.2	Numerical results		42
5	Con	clusion	ıs		45
\mathbf{A}	Cable array approach				48
В	3 Cost function			51	
Bi	bliog	raphy			53

List of Tables

4.1	IEA 15 MW parameters	33
4.2	Comparison of optimization results for different wind farm sizes.	
	Lower LCOE values indicate better performance. RS values represent	
	the average over multiple runs	34
4.3	Simulation results. The initial layout features a LCOE of 177.612	
	EUR/MWh	43
A 1		
A.1	Checker grid configuration results. "OR." refers to the mathematical	40
	solver.	49
A.2	Smart start configuration results. "OR." refers to the mathematical	
	solver	49
В.1	Full cost function breakdown. The units of distance are differentiated	
	based on the case with subscripts: "d" indicates water depth, "s"	
	indicates distance from shore and "p" indicates distance from port.	51

List of Figures

2.1 2.2	Visualization of top-hat wake models	7 10
3.1	Workflow of the adopted iterative optimization approach	19
3.2	Three catenary mooring system cost dependency on water depth	23
3.3	Catenary mooring system [41]	23
3.4	PyWake components. "Engineering models" refers to wake deficit model and wake propagation method. Adapted from [34]	24
3.5	Section of a typical inter array cable [43]	25
3.6	Visualization of connection topologies	26
3.7	Lazy wave shape	27
4.1	National parks mapping in Sardinia [49]	30
4.2	12 sector wind rose	31
4.3	All sectors wind speed occurrence distribution compared to the Weibull fit	32
4.4	Bathymetry contour map. Adapted from [53]	33
4.5	Power and thrust coefficient of the IEA 15 MW	34
4.6	LCOE as a function of iterations, for 20 turbines (top), 44 turbines (middle), 66 turbines (bottom) cases	35
4.7	Solutions provided by COBYLA (left) and RS (right)	36
4.8	Percentile visualization	39
4.9	Sensitivity analysis results	40
4.10	12 sector wind rose	41
4.11	All sectors wind speed occurrence distribution compared to the	
	Weibull fit	41
4.12	Bathymetry contour map. Adapted from [53]	42
4.13	LCOE as a function of iterations	43
4.14	Solution provided by COBYLA (top left), RS1 (top right), RS2 (bottom left) and RS3 (bottom right)	44

A.1	Example of the two layouts, 20 turbines. The substation is shown	
	in red, while the turbines are shown in black	48

Acronyms

AEP

Annual Energy Production

CAPEX

Capital Expenditure

CERRA

Copernicus European Regional ReAnalysis

 \mathbf{CF}

Capacity Factor

CFD

Computational Fluid Dynamics

COBYLA

Constrained Optimization BY Linear Approximation

DECEX

Decommissioning Expenditure

DTU

Danish Technical University

$\mathbf{E}\mathbf{W}$

Esau-Williams

GA

Genetic Algorithm

HVAC

High Voltage Alternate Current

HVDC

High Voltage Direct Current

KPI

Key Performance Indicator

LCOE

Levelized Cost Of Electricity

NREL

National Renewable Energy Laboratory

NPV

Net Present Value

OPEX

Operational Expenditure

PSO

Particle Swarm Optimization

RES

Renewable Energy Sources

RS

Random Search

WACC

Weighted Average Cost of Capital

WFLOP

Wind Farm Layout Optimization Problem

Chapter 1

Introduction

Global warming represents for humanity one of the biggest challenges of the 21st century. It has undeniably been caused by human activities [1], and the development that they have seen since the industrial revolution. The reliance on fossil fuels, such as coal and oil, has powered societies since the 19th century, but at the cost of massive CO_2 emissions, which are rapidly warming the planet.

To counter this trend, the European Union has undertaken significant efforts to reduce greenhouse gas emissions and accelerate the decarbonization process, pursuing the large-scale deployment of renewable energy sources. In 2023, renewables accounted for 44.7% of total electricity generation, surpassing for the first time the share of fossil fuels [2]. Within the Fit for 55 package, the EU has also set the target of increasing the share of renewables to 40% of total energy production. Solar, wind and hydro energy are by far dominating the Renewable Energy Sources (RES) market, taking contributing to 38.5, 28.2 and 20.5 % of the overall electricity generation from renewable sources in 2023 [3].

Wind energy represents one of the most promising RES. In recent years, attention has progressively shifted from onshore to offshore installations, driven by higher resource availability offshore and the reduced impact on land use and landscapes. Nevertheless, offshore wind energy still faces economic challenges, with a higher cost of energy compared to onshore alternatives [4]. This factor drives the industry to develop technologies to reduce the investment costs, which represents the single biggest factor influencing cost of energy.

The offshore wind industry was initially lead by the development in shallow waters, especially in the North Sea, where fixed-bottom turbines can be deployed. However, in order to allow a wider adoption of the technology, a shift towards deeper waters is inevitable. Deeper waters render the fixed-bottom solution economically unfeasible, while floating turbines offer a valid alternative. The deployment of floating offshore wind farms poses technical, economic and environmental challenges. In a floating wind farm, several aspects affect the design, often requiring

compromises between different concurring phenomena. Energy losses due to wake interactions are more important when aerogenerators are placed close to each other, pushing for an increase in farm sizes, but other factors, such as the Inter Array cable routing, present higher costs with increased farm size. The electrical connection of the turbines represents a relevant cost, taking up 8.4 % of a farm's lifetime costs [5]. Historically, the layout optimization problem has been performed disregarding the cable routing, due to the higher relevance of the energy production in the economics of a wind farm, and in a second phase, the electrical layout was designed. This approach, however, neglects the impact the farm layout on the cable routing. Solving the layout and cable routing optimization in a combined approach allows to reach a better solution, significantly reducing the electrical connection costs by clustering the turbines and accepting a small reduction in Annual Energy Production (AEP). The present thesis proposes a novel approach in the problem, implementing a cost function specifically designed for the construction of wind farms in the Mediterranean and optimizing the layout considering the Inter Array cable routing problem, in a sub-optimization approach. The framework is based on the open-source software TOPFARM [6] for the layout optimization routine, and on OptiWindNet [7] to solve the Inter Array cable routing problem. The framework is then applied to two case studies in Sardinia, a region that has attracted several floating offshore project developers. The first case, located near Rada di Alghero, represents a more economically interesting case, with a simple bathymetry. The case is designed to be eligible to support schemes promoted by the Italian government. Three sizes have been investigated, and the results commented. The second case study, located near the Asinara gulf, was designed to be a stress test, where the performances of the framework were tested in a more constrained environment, with a constraint on the maximum depth for the cable routing.

Chapter 2

State of the art

The spatial arrangement of wind turbines within a wind farm plays a decisive role in determining the overall performance of the system, influencing not only the energy yield, but also the operational and maintenance costs. The interdependence between turbines, primarily due to wake interactions, makes the WFLOP particularly challenging, as it requires a careful balance between aerodynamic, economic, and environmental considerations.

Research on WFLOP dates back to the pioneering work of Mosetti et al. [8] in 1994, which provided an early approach to the problem. More recent contributions have expanded the scope of the optimization process, integrating multi-objective formulations, higher-fidelity wake modelling, and different optimization algorithms.

The purpose of this chapter is to critically review the state of the art in WFLOP, with particular emphasis on three fundamental components of the optimization process. First, the definition of objective functions, which formalize the criteria to be optimized, ranging from the maximization of AEP to the minimization of the cost of energy, often incorporating multidisciplinary aspects. Second, wake modelling, which determines how the aerodynamic interactions between turbines are represented and thus directly affects the accuracy of energy production estimates. Wake effects typically cause a production loss of about 20 \% in an affected wind turbine, which can increase to as much as 70 % when turbine rows are aligned with wind direction [9]. Due to the complexity of the phenomenon, several wake models have been developed, and the choice of one model over another should be evaluated carefully, because of the deep influence on the quality of the solution. Finally, the optimization algorithms themselves, which constitute the strategy used to reaching a solution sufficiently close to the optimal one as quickly as possible. Due to the complexity of the problem, several strategies can be adopted, each with its drawbacks and advantages. Hybrid approaches are adopted in some instances, in an attempt of leveraging the strengths of different algorithms.

By analysing these three aspects in detail, this chapter aims to provide a

structured overview of the main approaches available in the literature, highlighting their advantages, limitations, and areas of application.

2.1 Objective function

In the context of optimization, the objective function represents the mathematical expression that expresses the quality of a candidate solution. In a WFLOP, the definition of the objective function is crucial, as it dictates both the optimization strategy and the modelling approach.

A significant portion of the literature adopts AEP as the primary objective [10],[11]. In this formulation, the optimization problem is treated as a single-objective maximization, where the goal is to position turbines in such a way that wake losses are minimized and the net energy yield is maximized. This approach provides a straightforward performance indicator. However, maximizing AEP alone may not fully capture the practical constraints and economic drivers of wind farm projects, such as foundation costs. When working with a multi-objective optimization problem, one could combine those functions into a single one through the application of weighting factors. For this reason, several works introduce techno-economic objective functions, which combine energy yield with additional metrics such as installation costs, yielding a single performance indicator that encompasses all. Typically, this indicator is the cost of energy, which can be either standard definition of LCOE [12],[13] (Equation 2.1) or it can be custom defined [8], but also the Net Present Value (NPV) is considered [14].

$$LCOE = \frac{CAPEX + \sum_{t=1}^{n} OPEX_{t}}{\sum_{t=1}^{n} \frac{AEP_{t}}{(1+r)^{t}}},$$
(2.1)

here "CAPEX" represents the capital expenditures, "OPEX" represents the operational expenses, "r" represents the discount rate and "n" represents the (expected) lifetime of the project.

Both LCOE and NPV require additional economic parameters, such as the discount rate, lifetime of the project and, only for NPV, electricity cost. The choice of these parameters effectively changes the outcome of the optimization significantly by changing the weighting factors [15], and as a result, an optimum found with a set of parameters will be different from the one found with another set. Therefore, those economic parameters should be as representative of the reality as possible. Due to the significant influence of these parameters on the economic parameters, it is advisable to perform a sensitivity analysis to evaluate the robustness of the results of the optimization.

In the scientific literature, several alternative objective functions have been proposed. Among the most common are the aerodynamic efficiency, defined as

the ratio between the AEP of the optimized layout and the AEP of the farm in the absence of wake effects, and the Capacity Factor (CF), given by $CF = \frac{AEP}{8760[h] \cdot P_{farm}}$, where P_{farm} denotes the rated power of the farm. It is important to note, however, that the maximization of either of these quantities is equivalent to the maximization of the AEP.

2.2 Wake models

A wind turbine's wake is the region downstream of the rotor where energy extraction by the turbine leads to reduced wind speed and increased turbulence compared to undisturbed air. The lower air velocity typically causes a 20% reduction [9] in power production with respect to undisturbed conditions, reaching higher values in the case of turbines alignment with the wind direction. Furthermore, the increased turbulence causes significantly higher mechanical loads on the turbine blades. The significance of the impact makes the accurate representation of the wake crucial for wind farm simulations.

The wake region is divided into two subregions: the near wake region (extending from about 2 to 4 rotor diameters downstream of the rotor plane) and the far wake region (beyond 4 rotor diameters downstream) [16]. There are various approaches to the modelling of a wind turbine wake, ranging from low-fidelity analytical models to high-fidelity Computational Fluid Dynamics (CFD) - based models. CFD models, whether RANS or LES, can capture the 3D structure of the velocity field in great detail, but their high computational cost makes them impractical for optimization studies. Therefore, due to lower computational costs , analytical wake models are usually preferred. In these models, the velocity deficit (δ) in the wake region (Equation 2.2) is obtained from different parameters, depending on the model, such as the distance from the rotor.

$$\delta(x, y, z) = \frac{U_{\infty} - U(x, y, z)}{U_{\infty}} \quad , \tag{2.2}$$

Here U_{∞} represents the free stream wind speed.

Due to their simple nature, analytical models are only valid in the far-wake region. However, this limitation does not compromise their applicability to wind farm modelling, since turbines are typically spaced several rotor diameters apart, placing them well within the far-wake zone.

A brief description of well-established one or two-dimensional models [9] typically adopted in wind farm modelling and optimization will follow in the next subsections.

2.2.1 Jensen

Suggested by N.O. Jensen in 1983 [17], the model consists of a 1D equation (Equation 2.3) which relates the velocity deficit, in the far wake region, to the distance from the rotor.

$$\delta(x) = 2a \left(\frac{D_{rotor}}{D_{rotor} + 2\alpha x} \right)^2, \tag{2.3}$$

Here α represents the entrainment factor, which in the 1983 paper was considered constant and equal to 0.1. In recent years, typically, the value is set to 0.075 in onshore sites and 0.04 in offshore sites. These updated values better capture the empirical observations.

This model is thus characterized by the assumption on the conical shape of the wake (Figure 2.1), which is commonly referred to as "top-hat". It is based on two hypotheses, the first one being the conservation of the cross stream integral of the velocity, and the second one being the distance from the rotor is the only parameters that affects the velocity deficit.

In case of multiple wakes, the combined effect is calculated by the quadratic sum, i.e. linear sum of the deficit in kinetic energy:

$$\delta_{overall} = \sqrt{\left(\sum_{i=1}^{N_{turb}} \delta_i^2\right)}.$$
 (2.4)

Jensen's model, while being one of the simplest available, represents one of the most present models in commercially available softwares (e.g. in the "PARK" model [18]) and is one of the most utilized models in scientific literature [19]. Its main strength is its very low computational cost and is rarely outperformed by other analytical models in AEP prediction [9]. The model is used in several works, including Mosetti's work [8] and Cazzaro et al. [14], where the aerodynamic model was used to yield an AEP prediction.

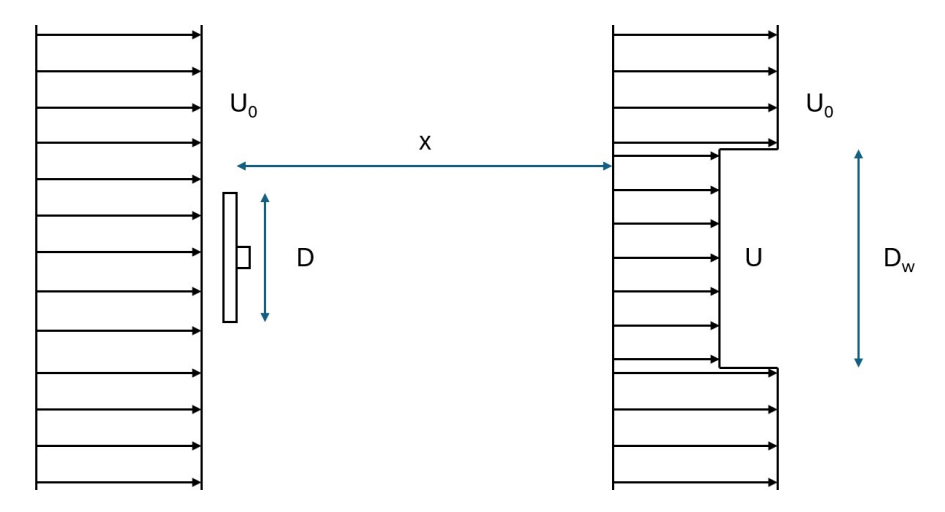


Figure 2.1: Visualization of top-hat wake models.

2.2.2 Frandsen

Frandsen's model is a 1-D wake model, developed by S. Frandsen et al. [20] in 2004. The model is based on the assumption that wind's momentum is conserved. By applying the conservation law, assuming self similarity and constant speed profile, it is possible to express the deficit δ as:

$$\delta(x) = \frac{1}{2} \left(1 \pm \sqrt{1 - 2\frac{A}{A_w(x)} C_T(U_{in})} \right). \tag{2.5}$$

Where the sign of \pm is determined by the value of the axial induction factor a in the turbine that generates the wake.

The wake area A_w has a diameter $D_w(x)$, which depends on three parameters, one of which is the constant k=2, as shown in Equation 2.6.

$$D_w(x) = D\left(\beta^{\frac{k}{2}} + \alpha \frac{x}{D}\right)^{\frac{1}{k}}.$$
 (2.6)

The wake expansion parameter β and wake decay constant α depend on the operating condition of the upstream turbine, and are defined respectively in Equation 2.7 and Equation 2.8.

$$\beta = \frac{1 + \sqrt{1 - C_T(U_{in})}}{2\sqrt{1 - C_T(U_{in})}},$$
(2.7)

$$\alpha = \beta^{\frac{k}{2}} [(1 + 0.1 \frac{x}{D})^k - 1] \frac{D}{x}.$$
 (2.8)

Frandsen's model also falls in the category of the top-hat models. In terms of performance, it shows a good overall correlation between measured and predicted power production, but is usually outperformed by Jensen's model [9].

O. Rahbari et al. in 2014 [21] used Frandsen's model in an onshore wind farm optimization, with the scope of minimizing the CoE.

2.2.3 Larsen

Larsen's model was developed in 1988 [22] and further improved in 2009 [23] by G.C. Larsen. Unlike the models described earlier in this chapter, Larsen's model is two-dimensional, as it also accounts for the radial distance from the centreline. Furthermore, the radial component of the perturbation is provided. The model is based on the thin shear layer approximation of the axis-symmetric RANS equations, assuming a uniform inflow speed. By assuming steadiness, axis-symmetry and self-similarity along the direction of the flow and by imposing two boundary conditions: speed continuity in the border of the wake $(u_x(x, r = r_w) = 0)$ and the assumption that the perturbation is significantly smaller than the inflow $(U_{\infty} >> u_x)$, the wake perturbation u_x and u_r for the axial and radial component respectively, and the wake's radius r_w can be calculated:

$$u_x(x,r) = -\frac{U_\infty}{9} (C_T A x^{-2})^{\frac{1}{3}} \left\{ r^{\frac{3}{2}} (3c_1^2 C_T A x)^{\frac{-1}{2}} - \left(\frac{35}{2\pi}\right)^{\frac{3}{10}} (3c_1^2)^{\frac{-1}{5}} \right\}^2, \tag{2.9}$$

$$u_r(x,r) = -\frac{U_{\infty}}{3} (C_T A)^{\frac{1}{3}} x^{\frac{-5}{3}} r \left\{ r^{\frac{3}{2}} (3c_1^2 C_T A x)^{\frac{-1}{2}} - \left(\frac{35}{2\pi} \right)^{\frac{3}{10}} (3c_1^2)^{\frac{-1}{5}} \right\}^2, \tag{2.10}$$

$$r_w(x,r) = \left(\frac{35}{2\pi}\right)^{\frac{1}{5}} (3c_1^2)^{\frac{1}{5}} (C_T A x)^{\frac{1}{3}}, \tag{2.11}$$

Where parameter c_1 is an empirically defined constant.

The absolute axial velocity can be then simply be calculated by adding the free stream velocity to the axial perturbation $U_w = U_\infty + u_x$. Equation 2.9, Equation 2.10 and Equation 2.11 are derived using the first order approximation. In [22], the solution to the second order wake model is provided. While providing a more complete model, the added terms provide marginal improvements in most of the engineering applications [16].

Improved model

In his 2009 paper [23], Larsen provided an improved version of the model by changing boundary conditions, properly calibrated with full-scale experiments

data, one imposed at the rotor plane and one at the distance of 9.6 diameters downstream. The resulting equations, with first order approximations, for the axial perturbation component and the wake radius are shown, respectively, in Equation 2.12 Equation 2.13

$$u_x(x,r) = -\frac{U_{\infty}}{9} (C_T A(x+x_0)^{-2})^{\frac{1}{3}} \{ r^{\frac{3}{2}} (3c_1^2 C_T A(x+x_0)^{\frac{-1}{2}} - (\frac{35}{2\pi})^{\frac{3}{10}} (3c_1^2)^{\frac{-1}{5}} \}^2, (2.12)$$

$$r_w(x,r) = \left(\frac{35}{2\pi}\right)^{\frac{1}{5}} \left(3c_1^2\right)^{\frac{1}{5}} \left(C_T A(x+x_0)\right)^{\frac{1}{3}},\tag{2.13}$$

Where

$$c_1 = \left(\frac{105}{2\pi}\right)^{-1/2} \left(\frac{d_1 D}{2}\right)^{5/2} (C_T A x_0)^{-5/6},$$

$$x_0 = \frac{9.6 D}{(2R_{9.6D}/(d_1 D))^3 - 1},$$

$$d_1 = \sqrt{\frac{1 + 1/\sqrt{1 - C_T}}{2}}.$$

The 2009 version also considers the case of superposition of wakes, providing two methods for adjusting to that case, as per hypothesis the inflow speed needs to be uniform. The first method is by considering the geometrical average on the surface:

$$\overline{U} = \frac{1}{A} \int_{A} U_{in} dA. \tag{2.14}$$

The second method is based on the rationale that the rotor thrust depends on the square of the velocity, thus justifying the averaging method in Equation 2.15:

$$\overline{U} = \sqrt{\frac{1}{A} \int_A U_{in}^2 dA}.$$
 (2.15)

B. Hwang et al.'s work in 2018 [24] makes use of Larsen's model combined with the Unsteady Vortex Lattice Method in a CoE optimization considering the inter-array electrical grid and water depth, using TOPFARM.

2.2.4 Bastankah and Porté-Agel

Already in his 1983 work Jensen [17] observed that the wake shape is similar to a Gaussian bell when comparing his model to measurements. One of the first Gaussian wake models is the one proposed by Bastankhah and Porté-Agel [25]. The model is based on momentum conservation and the wake deficit is assumed to follow a Gaussian distribution, regardless of the incoming conditions (Figure 2.2).

The governing equation is shown in Equation 2.16

$$\delta(x,r) = C(x)e^{-\frac{r^2}{2\sigma^2}},$$
(2.16)

where C(x) is the maximum deficit at the centre of the wake, defined as Equation 2.17

$$C(x) = 1 - \sqrt{1 - \frac{C_T(U_{in})}{8(\sigma/d_0)^2}},$$
 (2.17)

and the wake width σ is defined as Equation 2.18

$$\sigma = k * x + \epsilon * d_0, \tag{2.18}$$

Here ϵ is the wake expansion parameter, which in the 2014 paper is empirically set to 0.2β , and β is here defined as Equation 2.19

$$\beta = \frac{1}{2} \frac{1 + \sqrt{1 - C_T}}{\sqrt{1 - C_T}}. (2.19)$$

When the authors compared the model to LES data, they observed good agreement. The results show that the wake deficit profile can be assumed to have a self similar Gaussian shape after 3 rotor diameters from the upwind turbine [25]. A favourable feature of the Gaussian model is the reduced sensitivity on the wind direction with respect to top-hat models [25].

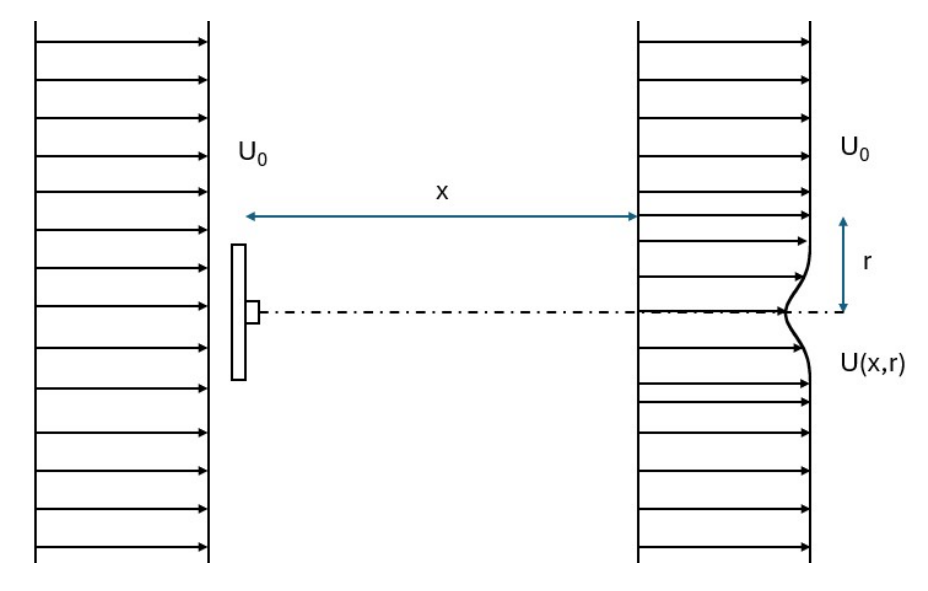


Figure 2.2: Visualization of Gaussian wake models.

In the work by K.S. Eikrem et al. in 2023 [12] where a wind farm is optimized with the scope of minimizing the LCoE, Bastankah and Porté-Agel's model is used. The authors point out the low computational cost of the aerodynamic model, performed on PyWake.

2.3 Optimization algorithms

Optimization is generally defined as "the process of identifying the best possible solution to a given problem" [26]. The WFLOP falls into the category of NP-hard optimization problems, characterized by a large search space and multiple constraints. Because of this complexity, exact methods are often impractical for real-world applications. For this reason, the literature has focused primarily on heuristic and meta-heuristic algorithms, which are able to provide high-quality solutions within reasonable computational times, even though they cannot guarantee the achievement of the global optimum. Other algorithms, based on local search, can also be found, although under-represented. The choice of the algorithm is also influenced by the variable's nature. Design variables can be discrete or continuos. Continuous variables are usually turbines position or the hub height. Discrete variables can be turbine type, or turbine's position, when the domain is divided into a grid.

The following section provides an overview of some of the most frequently used algorithms in the literature. It is worth noting that several algorithms can be combined to leverage the strength of different approaches and mitigating the drawbacks.

2.3.1 Genetic Algorithms

Genetic Algorithms (GAs) represent a class of meta-heuristic optimization algorithms inspired by the principles of natural selection and genetics. They are particularly valued for their ability to explore complex search spaces, find globally or locally optimal solutions, and their independence from function gradients, making them robust for problems with non-linear and non-convex objective functions.

Operating principle

A GA operates on a population of individuals (candidate solutions), each represented by a chromosome—an encoding of the design variables—composed of genes. The evolutionary process proceeds iteratively over generations through the application of key operators:

• Selection: Individuals with higher fitness values (i.e., better solutions according

to the objective function) have a greater probability of being chosen as parents for the next generation.

- Crossover: This operator simulates genetic recombination by exchanging segments of chromosomes between two parents to produce new offspring. Crossover is fundamental for exploring the solution space efficiently, as it combines successful traits from existing solutions.
- Mutation: Introduces small random changes to genes within a chromosome.
 Although occurring with a lower probability than crossover, mutation is essential for maintaining genetic diversity within the population, preventing premature convergence to local optima, and enabling the exploration of new regions of the search space.

The flow of the algorithm typically follows these steps:

- 1. Population initialization: A defined number of individuals is initialized, usually randomly;
- 2. Fitness evaluation: each individual's performance is evaluated with respect to the objective function;
- 3. Parents selection: a selection criterion, based on the fitness of the single, determines the set of parents
- 4. New generation's formation: via crossovers and mutations the parents individuals create a new generation, whose fitness is evaluated.

This cycle continues until a stopping criterion is met, such as a maximum number of generations or the achievement of a satisfactory fitness value, and the best performing individual is selected.

The genetic algorithm, together with its variations, is among the most used algorithm in the context of wind farm layout optimization [27], and is present in the first paper regarding the problem [8], where the algorithm was used to optimize the layout of a wind farm, in a grid configuration, with respect to a custom objective function.

2.3.2 PSO

Particle Swarm Optimization (PSO) is a meta-heuristic algorithm inspired by the collective movement of birds in flocks or fish in schools. In such groups, the trajectory of each individual is influenced both by its own past experience and by the social interactions with its neighbours. In an optimization problem, each candidate solution is treated as a particle travelling through the space (i.e. the variable space) with a given velocity.

Operating principle

The classical version of PSO's algorithm will be briefly described:

- 1. Initialization: a number of particles is generated with a random position and velocity;
- 2. Function evaluation: Each particle is evaluated and, if better than the previous values, the personal best (P_i) and/or the swarm's best (P_g) are updated;
- 3. Velocity and position updated: positions and velocity are updated according to Equation 2.20 and Equation 2.21 respectively.

$$x_i^{t+1} = x_i^t + v_i^t, (2.20)$$

$$v_i^{t+1} = \alpha v_i^t + \beta_i \gamma_1 (P_i - x_i^t) + \beta_g \gamma_2 (P_g - x_i^t).$$
 (2.21)

where t indicates the t-th iteration, and i indicates the i-th particle. α (inertia), β_i (cognitive coefficient) and β_g (social coefficient) are user-defined parameters. γ_1 and γ_2 are random numbers $\in [0,1]$.

Steps 2-3 are iterated until a stopping criterion is met, usually a maximum number of iterations or satisfactory convergence. The term $\gamma_c \gamma_3(x_i^t - P_g)$, where $\gamma_3 = R \in [0,1]$ randomly chosen and γ_c is a constant parameter, can be introduced to Equation 2.21 in order to preserve diversity in the group [28].

In the work of S. Chowdhury et al. [29], the PSO algorithm is employed to maximize efficiency by optimizing both the turbine layout and the rotor diameter, either at the level of individual turbines or for the entire wind farm.

2.3.3 COBYLA

Constrained Optimization BY Linear Approximation (COBYLA) is an optimization algorithm presented by M.J.D. Powell in 1994 [30]. It is a local-search, gradient-free trust region based optimization algorithm.

Operating principle

Starting from an initial guess, a simplex in the solution space of n+1 vertices is generated, where n is the number of variables in the problem. A linear approximation of the values of the objective function and constraint functions is generated and the optimisation of the linearised functions is performed inside the trust region. The size of the trust region is adaptively adjusted depending on the quality of the local approximation. The stopping criterion is applied on the minimum size of the trust region. A distinctive feature of COBYLA is its tolerance to temporary

constraint violations, which are allowed in order to improve the quality of the local approximation.

Being a local-search method, a key limitation of COBYLA is its strong dependence on the initial guess, which can significantly affect the quality of the final solution. Local-search algorithms present a faster convergence than heuristics and meta-heuristics in absence of local optima, although it is rarely the case in WFLOP.

Despite being much less used in literature than other methods, its presence indicates the validity of the method in improving COE with added load constraints [31] or when optimising rotor size [13].

2.3.4 Random Search

Presented by J. Feng and W. Z. Shen, the Random Search (RS) algorithm was first proposed in 2013 [32] as a refinement method to improve optimal solution found with other algorithms in discrete formulations.

Operating principle

Starting from an initial guess, the algorithm is initialized

- 1. Initialization: The objective function is evaluated for the initial solution;
- 2. Random move: A random turbine is moved by a random step size in a random direction;
- 3. Feasibility check: The new layout is checked for any constraint violation. If there are any violations, the move is discarded and the algorithm restarts with the random move;
- 4. Fitness evaluation: The new layout is evaluated, and if the performance is improved, the layout is updated.

The steps are iterated until a maximum number of iterations is reached, or if the elapsed time in the iterative process exceeds a user-defined limit. In a later work, in 2014 [11], the algorithm was improved with adaptive mechanism that aims at reducing the computational cost, by simply keep moving a turbine, if it improved in the previous iteration. The algorithm is really simple, both to understand and to implement, yet it is capable of improving significantly the solution obtained by other algorithms. The algorithm's sensitivity to the initial solution diminishes with sufficient iteration, thereby enabling its application as a solver. [11].

2.4 Concluding Remarks

The review clearly highlights that the performance of wind farm layout optimization strongly depends on the choice of the objective function, the wake model adopted, and the optimization algorithm employed.

Based on these findings, this thesis adopts the LCOE as objective function. LCOE provides a holistic measure of a project's cost-effectiveness, making it a robust metric for optimization. Additionally, it is often considered a Key Performance Indicator (KPI) in energy projects, allowing comparison with different competing technologies or projects.

Jensen's model is chosen as wake model, due to its balance of reliability and computational efficiency. Its accuracy in AEP prediction has been proven by evaluation studies [9] and its presence in most tools.

As for the optimization algorithm, no single optimization algorithm is universally accepted as superior. The Genetic Algorithm (GA) is the most commonly used strategy, as it effectively explores the solution space, albeit at a non-negligible computational cost. Additionally, RS has shown good performance in improving the solution. In the present thesis, Random Search algorithm will be compared to the local-search based COBYLA in solution quality and computational cost.

In the next chapter, a complete description of the proposed framework is presented.

Chapter 3

Methods

This chapter describes the methodology adopted for the optimization of a floating offshore wind farm, with particular focus on the co-optimization of the layout and cable routing optimization. The main purpose of this chapter is to provide a comprehensive overview of the tools and procedures used, highlighting the contribution of the proposed framework to the available solutions.

The chapter is divided into two sections: the first one is an overview of some tools capable of performing cable routing optimization and/or layout optimization. The second section introduces the methodological framework adopted for the optimization of offshore wind farm design, describing for each fundamental step the approach taken and the tools adopted.

3.1 Wind Farm Optimization Software

Several software were developed in recent years capable of solving the WFLOP, both from the academic and private sector. These tools aim at supporting researchers and project developers in planning or simulating a wind farm. In order to achieve this, these tools contain all steps necessary in the optimization process i.e. the energy production estimation, economic evaluation and optimization strategy.

A distinction criterion between software is the availability, i.e. whether the software is open-source or not, as commercial software do not allow the implementation of self-developed algorithms nor the modification of the available ones. Furthermore, commercial software do not disclose the methodology applied for solving the WFLOP to the general public. The informations in this section were gathered from the presentations given in the websites.

TOPFARM

TOPFARM is a Python-based tool developed by the Danish Technical University (DTU). The tool is based on the open-source library OPENMDAO [33] and wraps the PyWake package [34]. The tool is able to consider various design variables, continuous or discrete, such as turbine position and hub height, to perform the optimization. TOPFARM is divided into three modules, flow field simulation and energy (performed by PyWake), cost estimation and layout optimization. Several optimization algorithms and cost functions are pre-implemented in the software, and need few tuning parameters. Crucially, the cost functions implemented in the tool are outdated (the newest one dates back to 2018) and focuses on fixed-bottom offshore wind farms. It is possible to perform nested inter-array cable routing optimization, albeit in a simplified manner: the turbines are connected electrically with a non-capacitated minimum spanning tree algorithm, and the role of the substation is neglected. This approach does not allow a proper simulation of the electrical layout of the farm, as no consideration regarding the topology, constraints and export cables are possible.

FLORIS

FLORIS [35] is a Python-based tool developed by NREL and Delft University of Technology. The tool was primarily designed to model and optimize wind farm performance through wake steering and other control strategies, and it is part of a family of software, WETO software stack [36], each developed for a specific sector of the wind energy industry and supported by the U.S. Department of Energy. The tool allows the layout optimization, both in gridded and non-gridded domains, by means of a genetic random search algorithm, aimed at improving the energy production. FLORIS currently disregards any cable routing simulation and optimization.

Vind AI

Vind AI is a commercial software developed by Vind AI [37]. The tool was developed to assist in the project design and development phase, assisting in the resource assessment, layout optimisation, cable routing optimization and financial analysis. It also allows environmental analysis, such as noise or shadow flickering simulations, to assess the impact on the surrounding areas.

The tool features the inter array cable routing and export cable optimization, by optimising both the substation position and the inter turbine electrical connection, in order to drive down the impact of the electrical infrastructure on the investment costs. In the latest release, Vind AI allows the co-optimization of the farm layout and the cable routes, with export cables.

WindPRO

WindPRO is a commercial software developed by EMD [38]. The tool aims at assisting the design and development phase of a wind farm, from the resource assessment to financial evaluation. It has a modular structure, with different components for different aspects of the project development, allowing also the visualization of the turbines to assess the impact on the landscape. The "Energy module" allows the layout optimization, with the possibility of additional constraints such as noise or loads.

Regarding the cable routing layout, the "eGRID module" allows the design of the electrical connections and minimization of the electrical losses, based on the local wind data.

In WindPRO the layout and cable routing optimization problems are treated as separate problems, i.e. the layout optimization is independent from the cable routing. As highlighted in [14], this approach leads to sub-optimal configurations, as the layout of the wind farm influences the cable routing problem.

OpenWind

OpenWind is a commercial software developed by UL Renewables [39]. The software was developed to assist in the project development of a wind farm, e.g. in the assessment of the uncertainty in the resource assessment to the layout optimization, of vital importance for the financing aspect of the project. The software allows to consider logistical aspects and constraints, such as roads, waterways, and grid connection location. The software allows the estimation of the electrical layout cost, but the optimization of the system is not implemented.

3.1.1 Concluding remarks

From the review of the available tools it is clear that the co-optimization of the layout and cable routing is an active field, as only Vind AI recently added the possibility of performing it, while other open-source and commercial software, to the author's knowledge, do not perform a joint optimization of the cable routing and layout of wind farms. In the following section, a new framework, in which both problems are assessed in a simultaneous approach is proposed. A visualization of the workflow can be seen in Figure 3.1

The section is structured in five parts:

- 1. Mathematical definition of layout optimization and cable routing optimization problems;
- 2. Definition of the objective function, with an overview of the techno-economic cost model;

- 3. Methodology for the estimation of the energy yield and presentation of the adopted tool;
- 4. Description of the cable routing optimization approach, including the implemented algorithms;
- 5. Integration of the components into the overall optimization workflow.

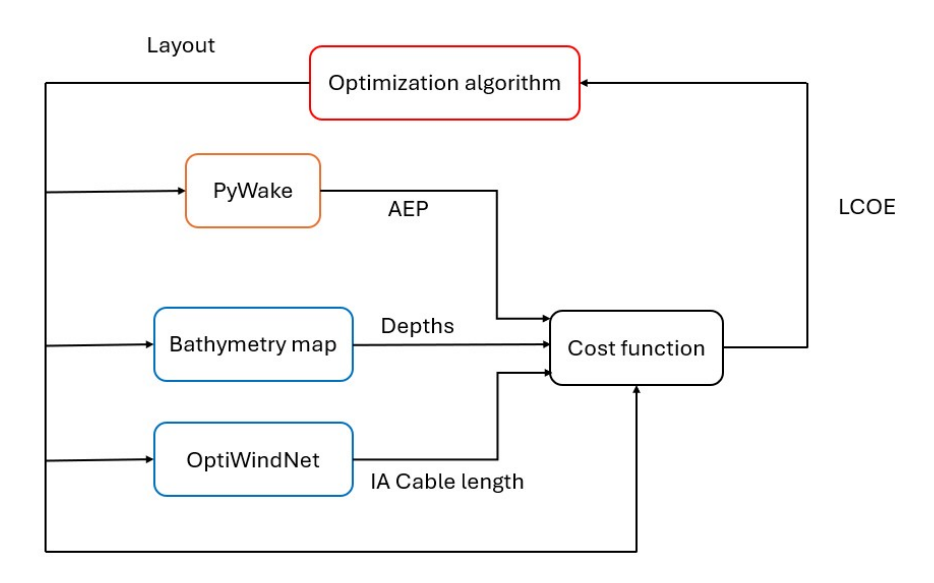


Figure 3.1: Workflow of the adopted iterative optimization approach.

3.2 Problem definition

The definition of the problem is formalized in the present section, as two distinct problems, for the layout and for the cable routing optimization.

3.2.1 Layout optimization

$$min\ LCOE(x_i),$$
 (3.1)

$$x_i \in \text{Boundary},$$
 (3.2)

$$x_{OSS} \in \text{Boundary},$$
 (3.3)

$$dist(x_i, x_j) \ge 5D \quad i \ne j. \tag{3.4}$$

The layout optimization problem is defined as the minimization of the LCOE Equation 3.1, with the turbines and substation positions inside a user-defined boundary (Equation 3.2 and Equation 3.3 respectively). Turbines are not allowed to be placed closer than 5 diameters distance (Equation 3.4) in order to keep aerodynamic loads within constructor's design limits. The turbines and substation positions are defined by two coordinates, treated as continuos variables.

3.2.2 Cable routing optimization

In this thesis, the optimization of the electrical layout is treated as sub-optimization, i.e. the electrical layout optimization is nested inside the turbines' layout optimization, and each iteration the cable routing problem is solved as discussed in subsection 3.2.2. Therefore, the algorithm will optimize the connection between turbines with their position and the substation's position as input.

To define the cable routing optimization problem, the parameter $y_{i,j}^k$ needs to be defined. It represents the decision variable for connecting the turbine i to the turbine j with a capacity of k. The substation is indicated with the subscript "s". The power flowing through the cable is indicated with " $f_{x,y}$ ". "T" indicates the set of turbines, while "S" indicates the set containing the substation.

$$y_{i,j} \in \{0,1\},\tag{3.5}$$

$$min \quad l_{IA \, cables}, \tag{3.6}$$

$$f_{i,j} \le 90 \left[MVA \right] \quad \forall i, j, \tag{3.7}$$

$$\sum_{i} y_{i,j} = 1 \quad \forall i, \tag{3.8}$$

$$\sum_{i} y_{i,j} \le 1 \quad \forall j, \tag{3.9}$$

$$\sum y_{s,i} = 0 \quad \forall i, \tag{3.10}$$

$$\sum y_{i,j} + \sum y_{m,n} \le 1 \quad \forall (\{i,j\}, \{m,n\}) \in C.$$
 (3.11)

The minimization of the overall length of the inter array cables (Equation 3.6) is achieved through the optimization of the cable routing, with a set of constraints. The first constraint is due to the radial topology, forcing every turbine to have only one exiting (Equation 3.8) and at most one entering cable (Equation 3.9), effectively connecting every turbine with a string. In case of branched topology, the condition in Equation 3.9 is relaxed. Equation 3.8 also forces the connection of every turbine. The substation is only allowed to have entering cables (Equation 3.10). The constraint in Equation 3.7 limits the apparent power flow in the cables. Lastly, cables are not allowed to cross each other's path (Equation 3.11), where C indicates the set of the available routes that cross each other.

3.3 Objective Function

The objective of the optimization is the minimization of the LCOE, as defined in Equation 3.12.

$$LCOE = \frac{CAPEX + \sum_{t=1}^{n} \frac{OPEX_{t}}{(1+r)^{t}} + \frac{DECEX}{(1+r)^{n+1}}}{\sum_{t=1}^{n} \frac{AEP_{t}}{(1+r)^{t}}},$$
(3.12)

where "n" represents the lifetime of the project, assumed to be 25 years, "r" represents the discount rate, assumed to be 6.61 % [40], and "DECEX" represents decommissioning expenses. LCOE is a measure of the cost of energy over the lifetime of the projects. It represents the fixed price at which the commodity should be sold in order to recover all the expenses at the end of the life of the project. The lower the LCOE, the more profitable the project.

CAPEX is assumed as a lump sum payment in the first year, DECEX are assumed to be paid in the first year after the end of operation (i.e. for a 25 years lifetime, CAPEX is considered in the year 0, DECEX is considered in the 26th year).

In order to estimate the expenditures, an appropriate cost function is needed. In this thesis, the cost function used is presented by S.A. Sirigu's work "Mapping the Levelized Cost of Hydrogen from Offshore Wind: A Case Study in Italian Waters" (forthcoming publication), where a cost function for the construction and installation of a floating offshore wind farm is derived from data found in the literature and from commercial projects, with a bottom-up approach. A detailed breakdown of the cost function is provided in Appendix B.

A contribution of Sirigu's study is the estimation of the cost of the mooring system of the turbines as a function of water depth. Taking the cost of a three-line catenary system (Figure 3.3) at 100 meters depth as reference C_{ref} , the cost at a generic depth h is obtained by applying a correction factor, as expressed in Equation 3.13:

$$C_{mooring} = C_{ref} \cdot f(h). \tag{3.13}$$

The correction factor f(h) is obtained by the look-up table and it is represented as a piece-wise function in Figure 3.2.

In Sirigu's work, the length of the Inter Array cables l_{IA} is assumed to be a function of the number of turbines n_t and their rotor diameters D ($l_{IA} = 1.125 \cdot n_t + 1.055 \cdot D - 122.64$). In the present thesis, this estimation was neglected, as the Inter Array cable length was calculated as described in section 3.5. One limitation of the cost function is the independence of the cost of the export cable from the rated power of the farm. This aspect effectively neglects the (significant)

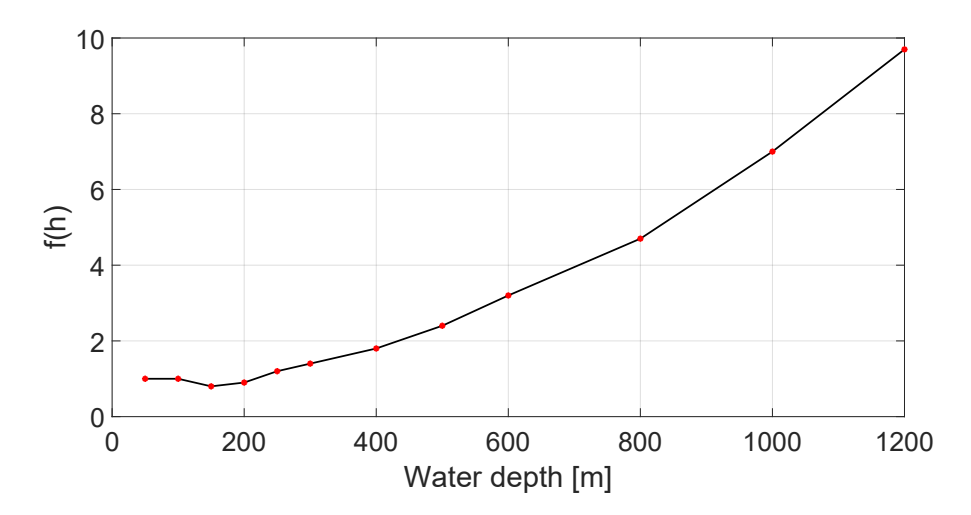


Figure 3.2: Three catenary mooring system cost dependency on water depth.

dependence of the export cable technology on the power flow, as for higher power outputs higher voltages or bigger sections are required.

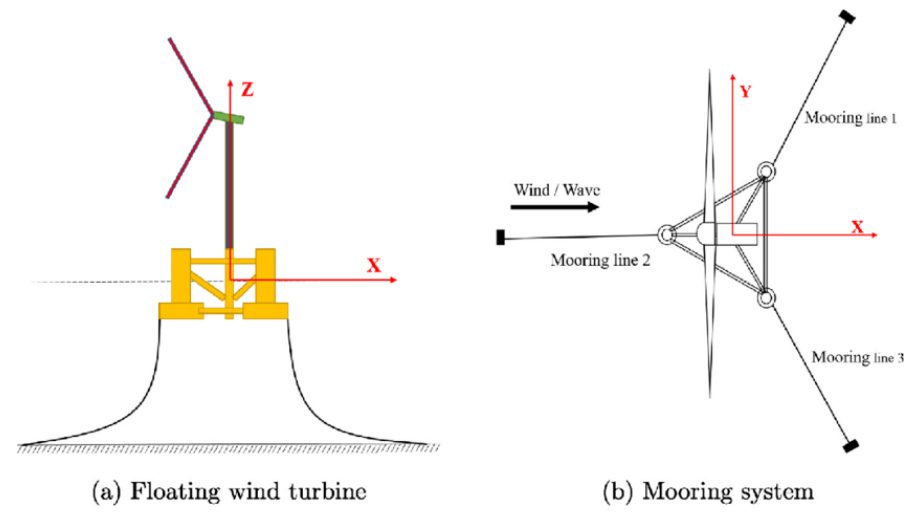


Figure 3.3: Catenary mooring system [41].

3.4 Annual Energy Production estimation

The AEP estimation is performed by PyWake, an open-source Python-based tool developed by DTU [34]. This tool enables the computation of the flow field in a wind farm as well as the estimation of the AEP, through the integration of site information, turbine model and wind resource data.

The tool workflow can be summarized as follows. From a reference wind speed and direction, the site object provides local wind conditions for any point of the domain. The wake model object calculates the wind speed deficit, and the local effective conditions are taken in input from the turbine object to calculate power production and thrust coefficient. Wake propagation can be modelled either by a simple downstream approach or through iterative methods in order to account for blockage effects, i.e., the influence of downstream turbines on upstream ones. The process is performed for all direction bins and all wind speeds, and the probability-weighted average yields the AEP. The flow chart of the operations described above is shown in Figure 3.4. It should be noted that PyWake does not

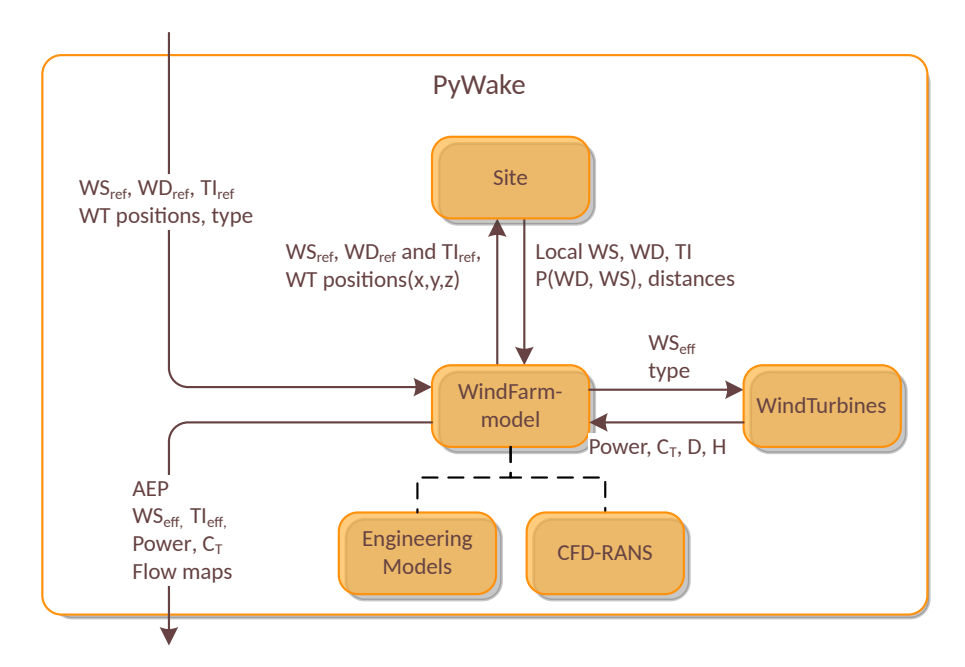


Figure 3.4: PyWake components. "Engineering models" refers to wake deficit model and wake propagation method. Adapted from [34].

simulate time-varying flow dynamics or complex wake interactions, which would require high-fidelity simulation tools.

In this thesis, due to the typical homogeneity of wind speed in offshore sites, wind speeds and directions were considered uniform along the domain. This assumption is common in literature [8][14][29].

Jensen's model (described in chapter 2) was chosen as wake model, as the low computational cost and good reliability make it the recommended model for layout optimizations [9]. Being it among the most represented wake models in literature [19], the choice is considered well justified. Blockage effects have been neglected, to avoid the need of iterations to calculate the effect on upstream turbines. This

simplification allows to reduce the computational cost of the workflow, at the cost of neglecting a phenomenon that impacts the power production in the order of few percentage points [42].

3.5 Inter Array cable routing

To define the Inter Array cable routing, OptiWindNet was used. OptiWindNet is an open-source, Python-based tool developed by DTU for optimizing inter-array cable routing within wind farms [7]. At the time of writing, the software is still under development, with the latest available release being version 0.0.7. In this work, version 0.0.4 was employed. This release enables the optimization of cable layouts by minimizing the total cable length. One of the key features of the tool is its ability to handle obstacle avoidance and crossing restrictions, automatically providing suitable detours in both cases.

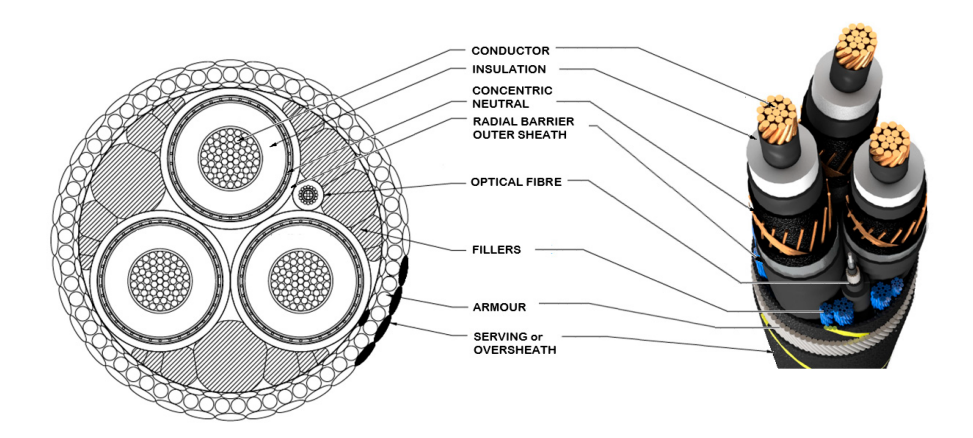


Figure 3.5: Section of a typical inter array cable [43].

Starting from the predefined turbine and substation locations, the tool is capable of optimizing cable routing by means of heuristics, meta-heuristics, or mathematical solvers. Mathematical solvers are algorithms that provide a guaranteed quality indicator, referred to as "gap", which expresses the relative difference (as a percentage) between the optimal solution and the one computed by the algorithm. Mathematical solvers are used via third party software. By default, the tool employs the CP-sat algorithm by Google OR-Tools software [44] as the mathematical solver; however, several alternative software, both proprietary and open-source, are also supported. In order to choose the mathematical solver, the performance of the open-source software have been investigated in two different layouts. For non-mathematical approaches, the tool currently implements two main algorithms: the heuristic Esau-Williams (EW) (including its modification) and a Genetic Algorithm-based

method. The EW algorithm was chosen over the meta-heuristic mainly for the advantage of not taking a user-defined amount of time, but it returns a solution as soon as available, although the Genetic Algorithm can achieve marginally higher quality solutions.

Given the nested optimization workflow, the main objective in selecting the algorithms was to minimize computational cost while still obtaining solutions of acceptable quality. For this reason, two approaches were compared: the exclusive use of the heuristic algorithm and the combined use of EW with a mathematical solver. The comparison considered both computational time and total cable length. The results of this analysis, presented in Appendix A, led to the selection of the EW heuristic alone due to the shorter computational time needed (in one case, EW was over 5 orders of magnitude faster).

Regarding the topology, two options are investigated, the radial (i.e. non-branched) layout, in which the substation is connected to the turbines through strings, each serving approximately the same number of turbines; and the branched topology, in which one turbine can connect to multiple turbines. The maximum number of turbines that can be connected to a single feeder depends on the rated power of the cables; in this work, a maximum capacity of 90 MVA per string is assumed (or six 15 MW turbines per string).

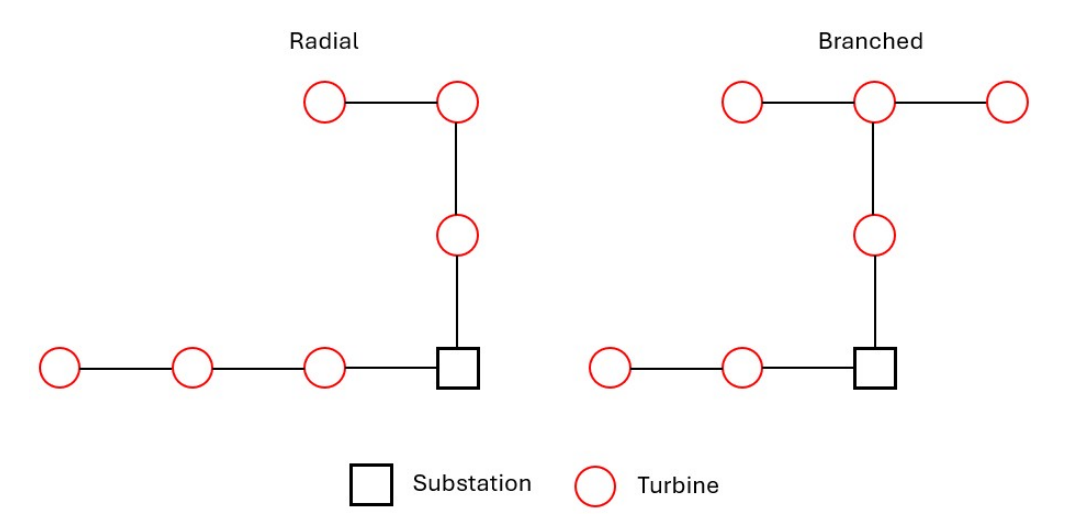


Figure 3.6: Visualization of connection topologies.

The classical approach for the Inter Array cable length calculation consists in calculating the euclidean distance between turbines to calculate the cable length, ignoring the added length due to water depth. In order to consider that, the dynamic cable route had to be modelled. Array cables are divided into two components, static cables, that are either buried or fixed to the sea bed, and dynamic cables, that connect the turbines to the static cables [5]. For deep waters (around 500

meters), the whole connection can be suspended, however, this configuration was excluded from the present study. Dynamic cables usually follow a "lazy wave" shape. While the exact length depends on the individual site, M.U.T. Rentschler et al. [45] suggested a generalized length of 2.8h, where h = d - 20 [m] and d is the depth of the water under the turbine. Furthermore, the position of the connection between the dynamic and the static part was assumed to be at a radial distance from the turbine of h. The geometry considered is shown in Figure 3.7.

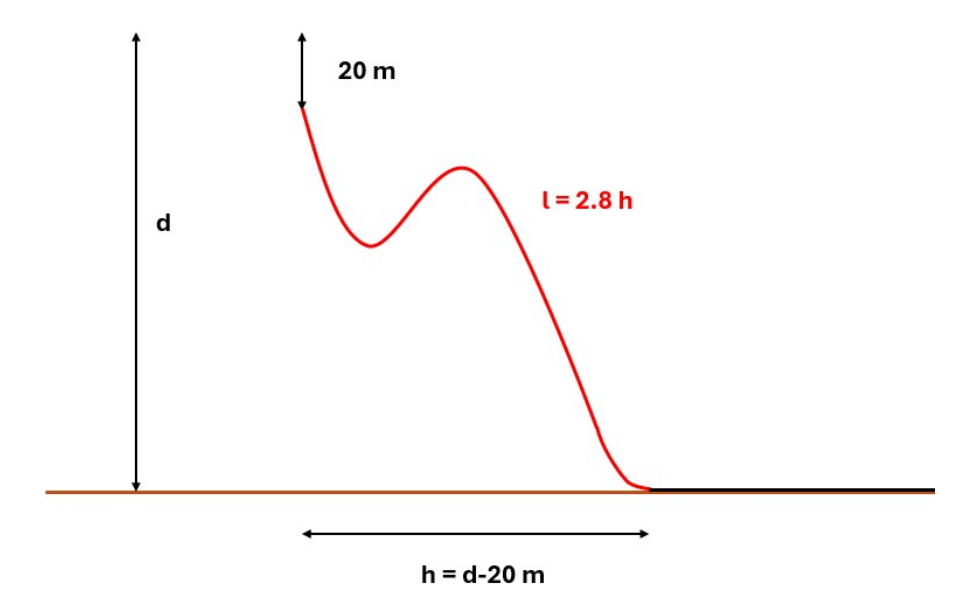


Figure 3.7: Lazy wave shape.

3.6 Optimization algorithm

The layout optimization was performed in TOPFARM, a Python-based tool developed by the DTU. The tool is based on the open-source library OPENMDAO [33] and wraps the PyWake package [6]. The tool is able to consider various design variables, such as turbine position and hub height, to perform the optimization. In the present thesis, two design variables were considered: turbine coordinates and substation coordinates. A single substation was considered, independently from the farm size. In more recent projects, the nominal power of the substations has increased up to more than 1 GW both in HVDC [46] and in HVAC [47] technologies. It is worth noting that, in case of bigger sizes, more substations should be added, which would require some modifications in the objective function to properly consider the plurality of export cables.

Two iterative algorithms were compared, COBYLA and RS, both previously

described in chapter 2. Since the original RS implementation accounts only for turbine coordinates, a modification was introduced to also optimize the substation location. With respect to the original algorithm, an additional step was added: at each iteration either a turbine position or the substation position is randomly perturbed, with the same average probability of modification. The constraint on the substation position was not handled by TOPFARM, but a penalty on the LCOE was applied when the substation was brought outside of the boundary. The value of the penalty is high, so that, effectively, the constraint is always respected.

Both COBYLA and RS need a good quality initial guess. In order to obtain it, the Smart Start Algorithm [48] is employed.

Smart Start is a greedy algorithm specifically developed to prepare an initial guess for the WFLOP. The algorithm operates by discretizing the domain into a grid and iteratively placing turbines. At each step, all feasible grid positions for the next turbine are evaluated and ranked in descending order of performance. The algorithm evaluates the performance of the layout by computing the LCOE, with a few simplifications: firstly, the inter array cable length is calculated with the minimum spanning tree algorithm, secondly, the substation is always placed in the centre of the layout (i.e. the coordinate is the average of the turbines' coordinates). These two simplifications are caused by the position of the substation being yet undefined. Its inclusion would presumably slow down the algorithm considerably without providing meaningful improvements to the quality of the initial guess.

To introduce an element of randomness, a parameter $random_{pct}$ can be introduced. The parameter determines the share of the highest performing positions, among which one is randomly chosen. However, in the present thesis, this parameter will be set to 0, effectively rendering the algorithm deterministic, to investigate the best performing layout.

Smart Start is highly sensitive to the grid resolution, as finer grids yield better results but increase also the computational time. Given the scope of the algorithm in the present work, a relatively coarse grid (around 10 diameters of spacing between points) is deemed sufficient, as the layout will be further optimized by the other algorithms.

The substation's initial position is not directly initialized by Smart Start, but it is determined by the centre of the turbine's layout, after it is defined by the Smart Start algorithm.

Chapter 4

Case study

The presented methodology was applied to two case studies, both located off the cost of Sardinia. The island represents an interesting area for wind projects, due to the availability of resource and presence of good electrical grid infrastructure. Currently, several projects are being investigated and are going through the bureaucratic path to get approved and begin construction. Most of these projects are being met with fierce opposition from the local population and institutions, as the relatively uncontaminated environment represents a key feature of the identity of the region. It is worth noting that, in the design of a wind farm, several non-technical aspects should be included in the project development, such as relations with the local residents and landscape impact. Protected marine areas and national parks, shown in Figure 4.1, should be excluded during site selection. These consideration were disregarded in the present thesis, but it is worth remembering that these aspects influence deeply the development of a project.

The simulations for the case studies were performed on a laptop featuring a 8^{th} generation i5 core operating at 1.60 GHz, 8 GB RAM.

4.1 Rada di Alghero

The site investigated in the case study is located off the west coast of Sardinia, south of the Rada di Alghero. This area is particularly relevant due to both the high wind resource and the availability of ports suitable for hosting construction vessels, an essential element in the logistics of project realization. Alghero's port will be taken as the reference port for the construction vessels cost calculation, as appointed as capable of hosting construction vessels by Sirigu. The straight-line distance between the port and the project site is 36.7 kilometres. The area is already attracting commercial interest, with several offshore wind projects under development. Notably, the Sardinia NorthWest project, by Hexicon S.r.l., is

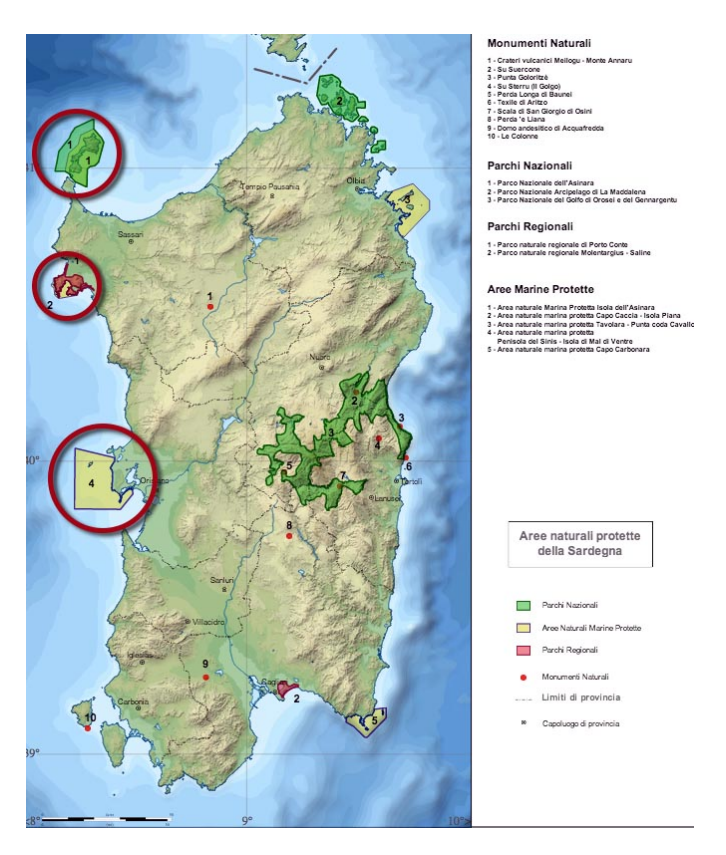


Figure 4.1: National parks mapping in Sardinia [49].

currently in the authorization phase and located in close proximity to the present case study site [47].

For the purpose of the case study, a constraint of distance from shore was taken from the "FER2" decree issued by the Italian environmental and energy security ministry. This decree, designed to promote renewable energy technologies with generation costs higher than market prices, stipulates that floating wind farms must be located at least 12 nautical miles (approximately 22.3 kilometres) from the coast in order to qualify for a Contract for Difference scheme, guaranteeing a fixed energy price of 185 EUR/MWh [50]. The coordinate of the reference point of the farm: 40.287530°N, 8.070366°E.

4.1.1 Environmental data

Wind data were retrieved from the Copernicus European Regional ReAnalysis (CERRA) product [51]. It offers a quite fine spatial resolution (5.5 km side grid) compared to other reanalysis products, though at the expense of lower temporal resolution, as data are made available every three hours. As the name suggests,

CERRA provides data for the European region. The reliability of the data provided is higher over simple terrain [51]. Wind speed and direction data are available at the chosen turbine's hub height, thus avoiding the need of estimating the resource at a different height from the measured. Reanalysis products such as CERRA are particularly useful for wind resource assessment, since they provide consistent, long-term, and uninterrupted datasets, and their validity for this application has been demonstrated. However, CERRA has shown a tendency in overestimating the resource [52], and should therefore be used in conjunction with local measurements to correct the bias, if higher accuracy is needed.

The years from 2000 to 2021 were used to assess the resource (22 years of reanalysis data), in the closest point to the reference point of the farm. The wind rose is shown in Figure 4.2. The resulting all-sector wind speed average is of 6.56 m/s or power density of $392 \, \text{W/m}^2$. Figure 4.3 shows the occurrence of the all sector wind speed occurrence distribution, showing a good fitting of a Weibull curve, justifying the use of a Weibull curve approximation of the resource.

The primary wind direction is along the NW-SE axis, accounting for nearly half of all occurrences, with 31 % from Northwest and 18 % from Southeast.

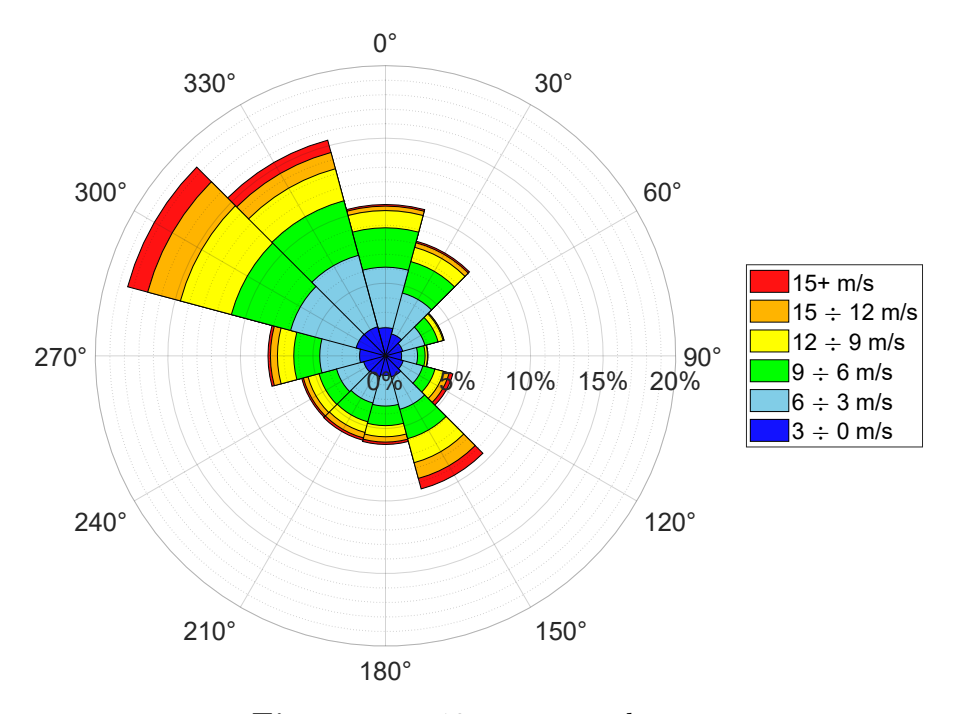


Figure 4.2: 12 sector wind rose.

Bathymetric data were retrieved from EMODnet. European Marine Observation and Data Network (EMODnet) is an european marine data service, that provides access to several marine data, among which bathymetry, seabed substrate and biological data [53]. For this case study, bathymetry data were gathered by different

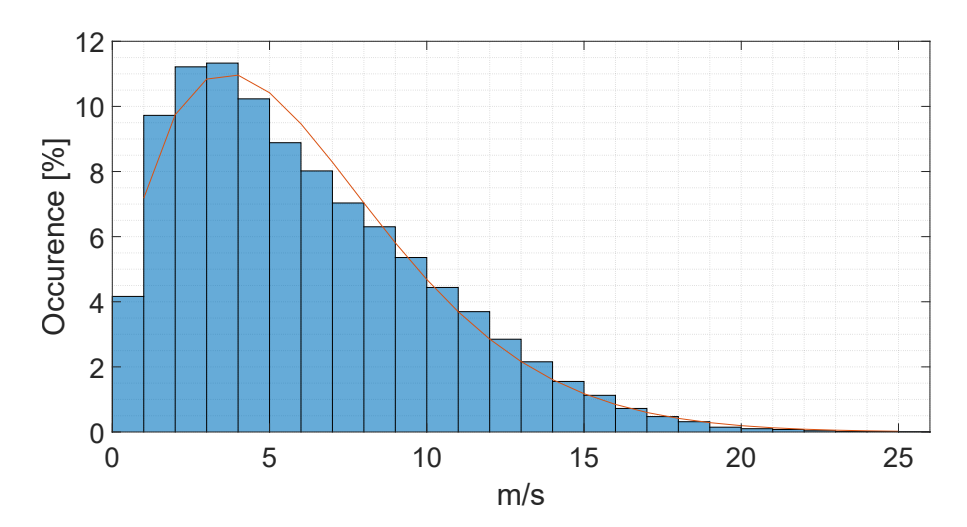


Figure 4.3: All sectors wind speed occurrence distribution compared to the Weibull fit.

providers ([54],[55],[56]). The raster data provided are gridded in a 1/16*1/16 are minutes grid (115x115 meters ca.). The bathymetry data was also used to retrieve the coordinates of the shore, from which the east boundary of the farm is obtained.

The site is characterized by relatively simple bathymetry. On the eastern side, the seabed is fairly flat, whereas the western boundary is marked by a steep depth gradient leading to an area exceeding 1200 meters in depth. Conversely, variations in depth along the north-south axis are minimal.

4.1.2 Wind turbine model

The chosen wind turbine model for the case study is the IEA 15 MW, a reference turbine designed by National Renewable Energy Laboratory, DTU and University of Maine in the context of the IEA Wind Task 37 in 2020. Reference turbines are publicly available designs of turbines, in programs of research, development and demonstration (RD&D) and usually are conducted with the collaboration of several actors of the industry, as well as researchers from universities.

The selected turbine model is able to reach a maximum of 30.74 % of capacity factor or 39 GWh annually in the selected site.

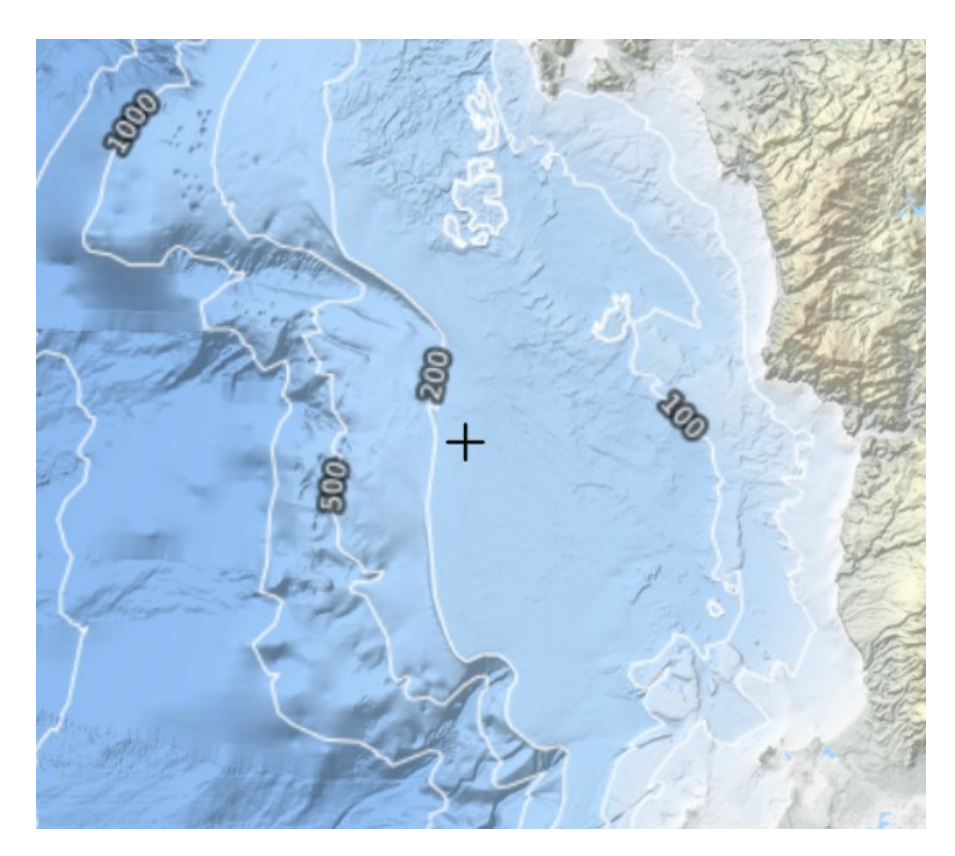


Figure 4.4: Bathymetry contour map. Adapted from [53].

Parameter	Value	Unit
Rated Power	15	MW
Rotor Diameter	240	m
Hub Height	150	m
Cut-in	3	m/s
Cut-off	25	m/s
Rated speed	10.59	m/s
Electrical efficiency	96.55	%

Table 4.1: IEA 15 MW parameters.

4.1.3 Numerical results

Three farm sizes have been simulated (20, 44 and 66 turbines), and for each configuration the performance of the two optimization algorithms have been analysed. The two algorithms present a significant difference: COBYLA is a deterministic algorithm, i.e. the result will be the same if the initial layout is identical, while RS is based on a stochastic approach. Consequently, three RS runs were performed for

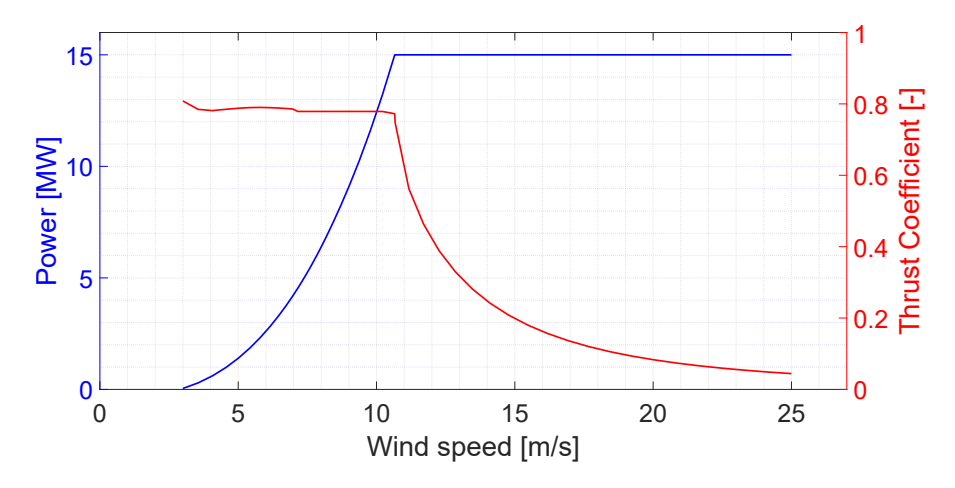


Figure 4.5: Power and thrust coefficient of the IEA 15 MW.

each case, while a single COBYLA run was sufficient for evaluation. In COBYLA, a tolerance of $1 \cdot 10^{-6}$ was used as stopping criteria. The comparisons were made with matching number of iterations, determined by COBYLA. The LCOE graphs (Figure 4.6) for COBYLA has been filtered to allow a good visualization, since the penalty term would otherwise make the results unreadable.

Parameter		COBYLA	1		RS	
No. of turbines	20	44	66	20	44	66
No. of iterations	1145	3973	8133	1145	3973	8133
Initial LCOE [EU-	168.884	168.574	169.951	168.884	168.574	169.951
R/MWh						
Improved LCOE	168.093	167.390	169.032	167.473	167.103	168.840
[EUR/MWh]						
Delta [%]	0.44	0.70	0.54	0.78	0.85	0.65
Time per iteration	0.32	0.71	1.18	0.39	0.87	1.41
[s]						

Table 4.2: Comparison of optimization results for different wind farm sizes. Lower LCOE values indicate better performance. RS values represent the average over multiple runs.

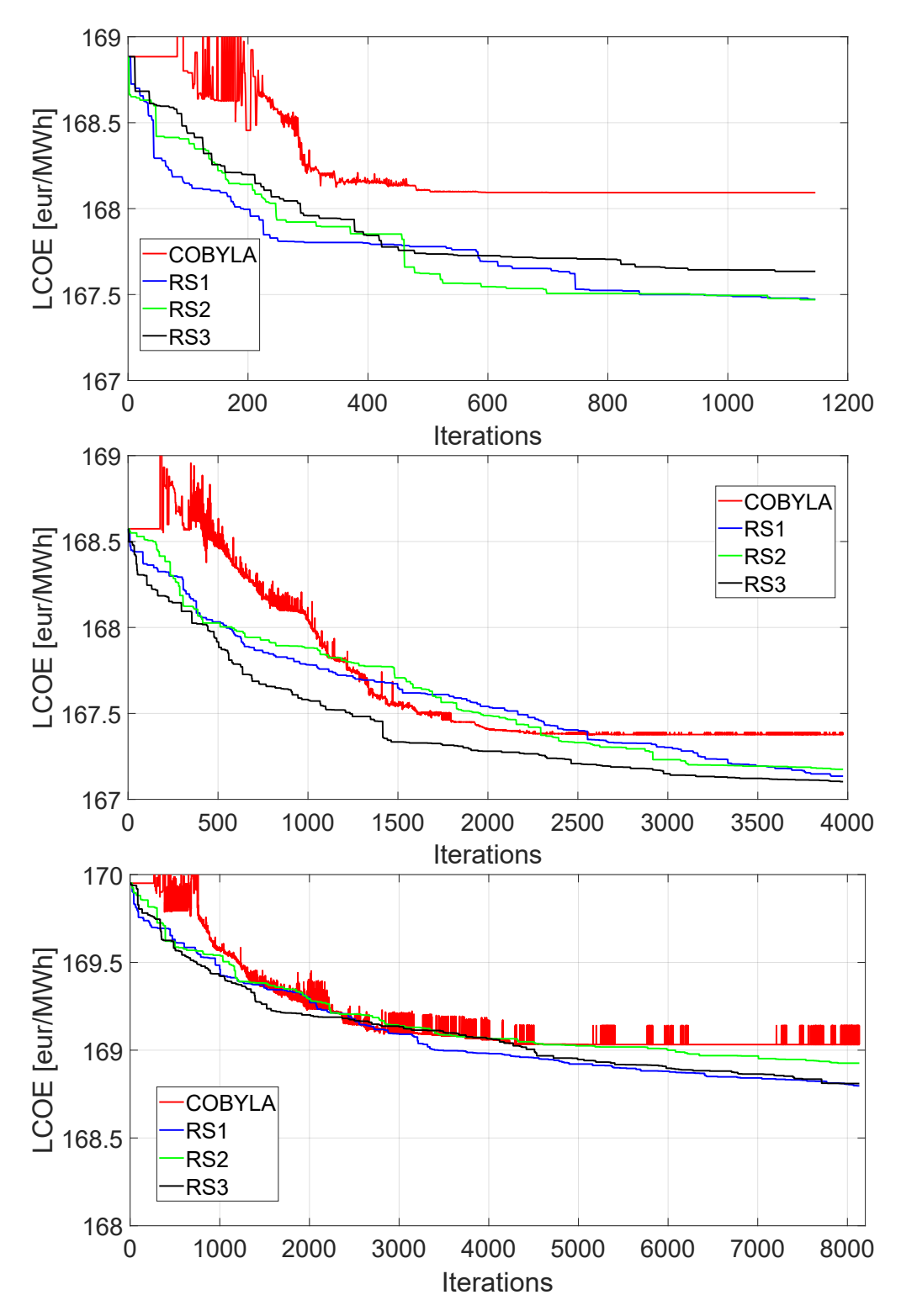


Figure 4.6: LCOE as a function of iterations, for 20 turbines (top), 44 turbines (middle), 66 turbines (bottom) cases.

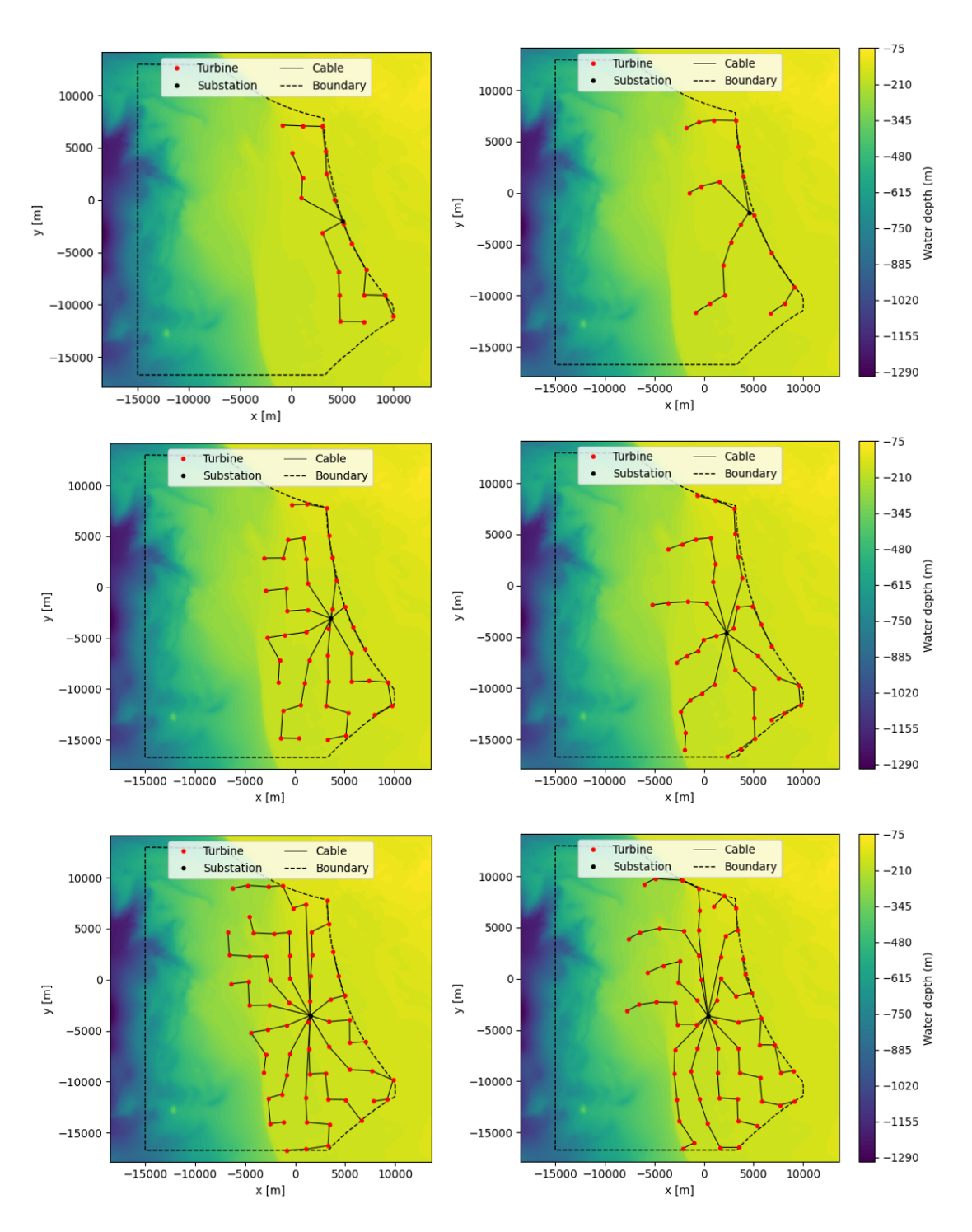


Figure 4.7: Solutions provided by COBYLA (left) and RS (right).

The results clearly highlight the superiority of the RS method in improving the layout generated by the Smart Start algorithm when compared to COBYLA, across all farm sizes. The local-search algorithm showed low effectiveness in changing significantly in the overall layout, effectively only changing the substation position in the 20 turbines case, while RS meaningfully re-arranges the layout and achieves a lower LCOE in all cases. It may be possible that COBYLA remains trapped in a local optimum layout from which it is not able to escape. Nonetheless, on average, RS required approximately 20 % more elapsed time per iteration with respect to its counterpart. The resulting layouts for each case are shown in Figure 4.7.

In the 20 turbines case, both algorithms are primarily driven by the minimization of the export cable length, due to its relative weight on the CAPEX. For the 44 and 66 turbines case, the export cable is less relevant, as more strings of Inter Array cable are present. As a result, the export cable length is not minimised and the substation is located closer to the centre of the layout. In both the 20 and 44 turbine scenarios, it is possible to observe a tendency towards row alignment perpendicular to the prevailing wind direction. This configuration minimizes wake losses under the most frequent flow conditions. In the 66 turbine case, however, this trend does not hold. Furthermore, turbines located near the centre of the layout do not display the streamlined structure observed in smaller farms, but instead preserve the initial checker board arrangement. This behaviour may suggest that certain optimization parameters (e.g., substation frequency or maximum step size) require further tuning.

Among the three cases, the 44 turbines size farm features the lowest LCOE, thus being the most profitable project. Compared to the 20 turbines layout, it features a slightly lower capacity factor (-1.3 %) but also a lower specific CAPEX (-1.5 %). The reduction in energy production is compensated by the more efficient exploitation of shallower areas, where lower installation costs are required. In the 66 turbine scenario, the layout requires a higher concentration of turbines in the shallow water area, which leads to a slight reduction in energy production (-1%) while maintaining the same specific CAPEX. This outcome suggests a saturation effect: beyond a certain farm size, the advantages of exploiting shallow areas may be offset by the increased wake interactions among turbines.

Sensitivity Analysis

In commercial projects, sensitivity analysis investigates how robust a project is with respect to changes in a single parameter—usually economic—that was initially based on assumptions. A good analysis should focus on the uncertain parameters expected to have the greatest impact on the results of the economic evaluation, and their value should not be arbitrary, but it should be based on historical data or projections. This analysis is performed in order to assess the risk that the

investors are taking on. Risk is a key factor in the financing phase, where the project developers seek financing from banks. Higher project risk generally leads to higher interest rates on loans. In this section, the sensitivity of the project's economic performance to three key parameters is analysed: discount rate, project lifetime, and power production.

Sardinia is characterized by recent hostilities towards renewable energy projects, due to a large number of factors. These hostilities usually affect the project, increasing risk. With an increased risk, usually debt is more difficult to obtain and the cost of capital increases.

The discount rate is a way of quantitively considering the change of value of the money in time. Although inflation is also part of the consideration, it is important to remember that for private projects, the discount rate is directly correlated to the cost of the capital invested in the project. For this reason the discount rate is often equal to the Weighted Average Cost of Capital (WACC) in the investment payment. For simplicity, the nominal value will be considered, and tax shielding will be neglected. WACC is made up of two parts, debt and equity. Debt is the money loaned from an institution, usually a bank or an investment fund. These loans usually have low interest rates, but come with monitoring requirements from the lender institution and benefit from protection in case of bankruptcy. Equity is the capital that comes from the firm. Usually, the cost of equity is calculated as opportunity cost, i.e. the cost of not investing capital in another project. Knowing the cost of debt and equity, the WACC is calculated with the weighted average of the cost of debt and cost of equity according to their share in financing. Projects that are financed by debt are liable of a tax shield, meaning that part of income tax is deduced, to account the debt payment. For this reason, when calculating WACC, this should be accounted for.

$$WACC = \frac{E}{D+E}r_e + \frac{D}{D+E}r_d(1-T),$$
 (4.1)

where r_e and r_d are the cost of equity and debt respectively, E and D are the debt and equity, T is the corporate tax rate. However, in the present thesis, taxation was not considered in the economic evaluation.

From 2020 to 2024, the average WACC for European offshore merchant projects increased by 4 % [57], therefore a worst case scenario of 10.61 % will be used. The case study was designed to be eligible for a Contract for Difference support, which is expected to reduce the WACC of 2 % [57] with respect to merchant projects. The effect of this risk reduction on the WACC was however neglected, in order to have a conservative assessment. Best case scenario is 5 %, i.e. the value suggested by Sirigu in his work.

A project lifetime of 25 years was assumed, according to the FER2 decree [50]. However, commercially available 15 MW turbines, like the V-236 from Vestas

[58], are designed for a 30 years lifespan, while older farms were planned to last 20 years [59].

Lastly, the sensitivity on the resource is assessed. Assuming a Gaussian distribution of the annual mean power density, the 25th and 75th percentile are taken as worst- and best-case scenarios, respectively (Figure 4.8). This is the standard approach in the evaluation of a renewable energy project during the financing phase. It is worth noting that the probability of having the resource consistently take the value of the 25th percentile for the whole lifetime of the project is very low.

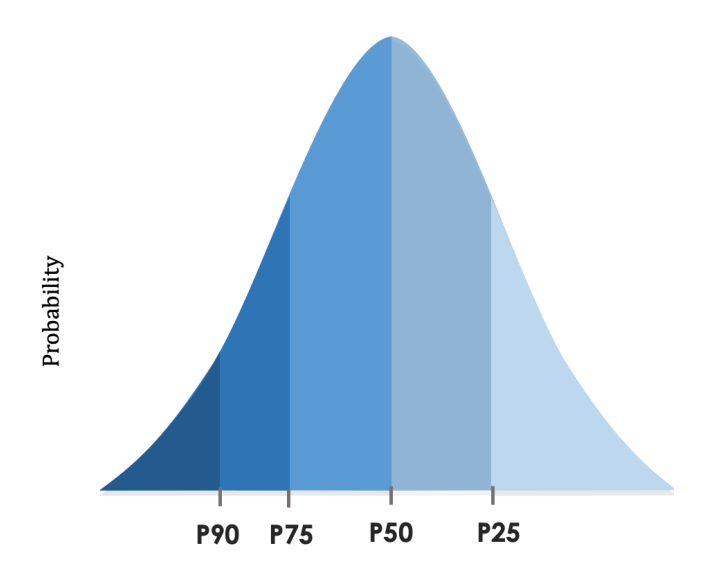


Figure 4.8: Percentile visualization.

The results of the analysis for the RS optimized 660 MW farm are shown in Figure 4.9.

As expected, the project is heavily sensitive to the discount rate. This is common for renewable energy projects, whose costs are mainly paid during the construction phase. With 10.61~% discount rate, the project is not profitable with the guaranteed price of $185~\rm EUR/MWh$.

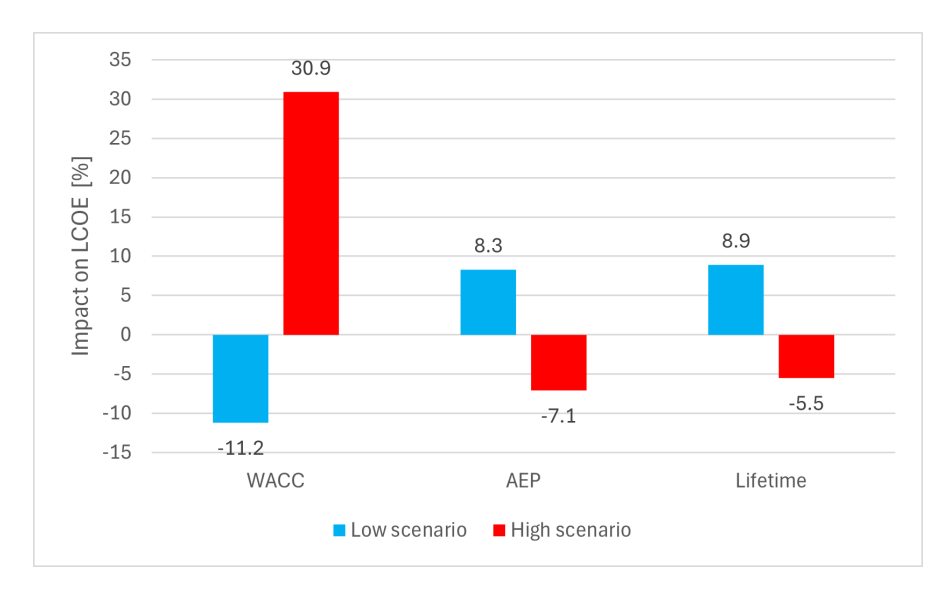


Figure 4.9: Sensitivity analysis results.

4.2 Asinara Gulf

The second case study is located off the north cost of Sardinia, in the Asinara gulf with the farm's reference point located at 41.1490°N, 8.6531°E. The area was interested by a construction proposal in 2012, when a wind farm of n. 28 3.6 MW turbines was proposed. The interest in the area highlights the good availability of the wind resource in the area. However, the area is located near a national park and protected marine area (marked as "1" in Figure 4.1), making the authorization of the project highly improbable.

The aim of this case study is to evaluate the framework's performance under more constrained conditions. In particular, a depth limit of 700 meters was imposed on the cable routing, with a branched network topology. Due to the scope of the second investigation, the constraint on the minimum distance from the shore was ignored, making the project ineligible to the support scheme. A single farm configuration was simulated, consisting of a 600 MW wind farm with 40 IEA 15 MW turbines.

4.2.1 Environmental data

The wind data used in the case study were retrieved from CERRA, in the cell closest to the reference point of the wind farm. The data come from the two year period of 2022 and 2023. The site is characterised by an average wind speed of 6.79 m/s and 478 W/ m^2 power density. The primary wind axis is East-West (E-W), accounting for a total of 31 % of all occurrences.

With the site's wind condition, the maximum yield of the IEA 15MW is 42.2 GWh, or 33.24 % Capacity Factor.

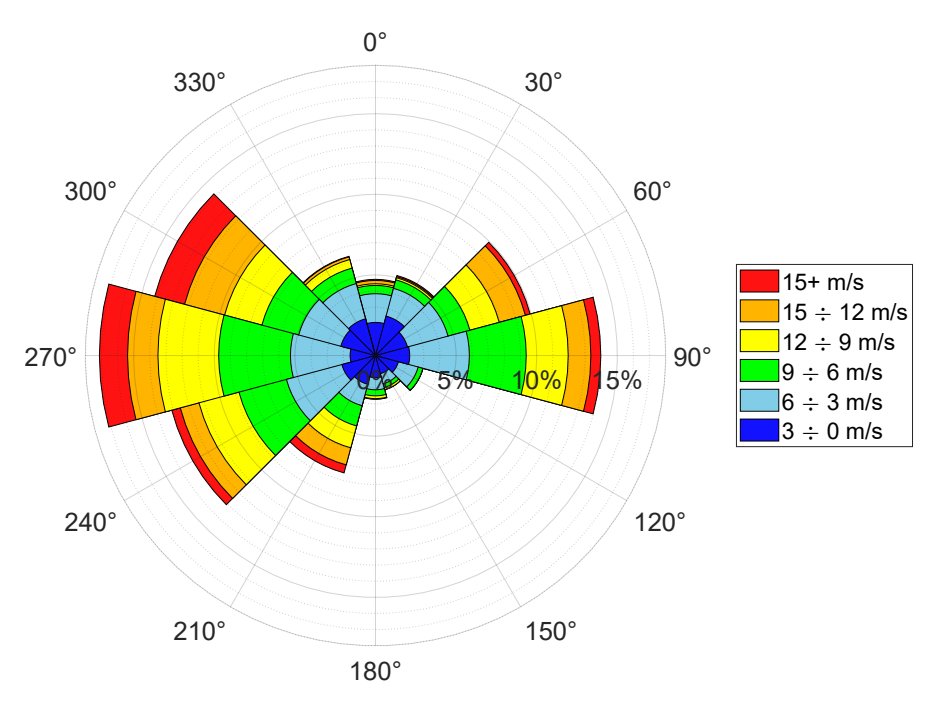


Figure 4.10: 12 sector wind rose.

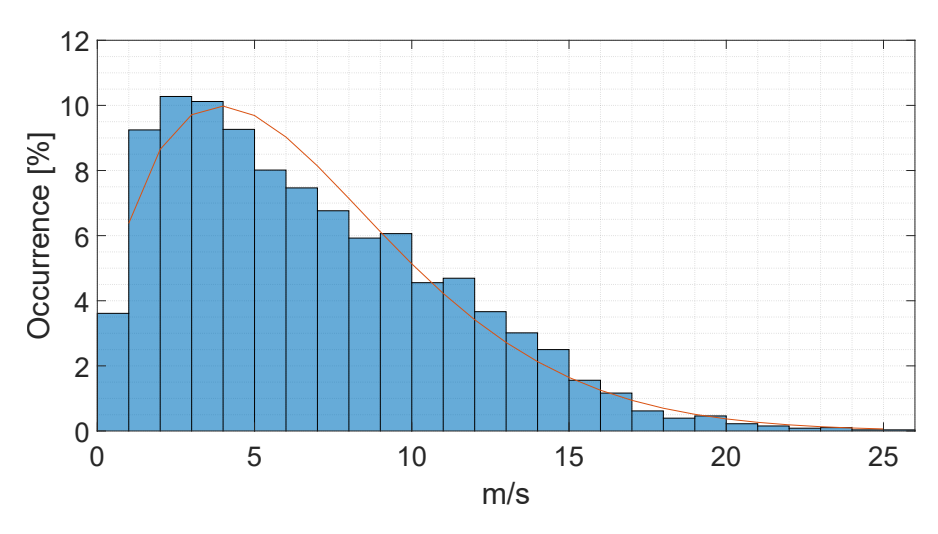


Figure 4.11: All sectors wind speed occurrence distribution compared to the Weibull fit.

Bathymetric data were retrieved from EMODnet [60]. The study area is characterized by plains of moderate depth (200–350 meters) separated by strips of deep

water (> 800 meters).

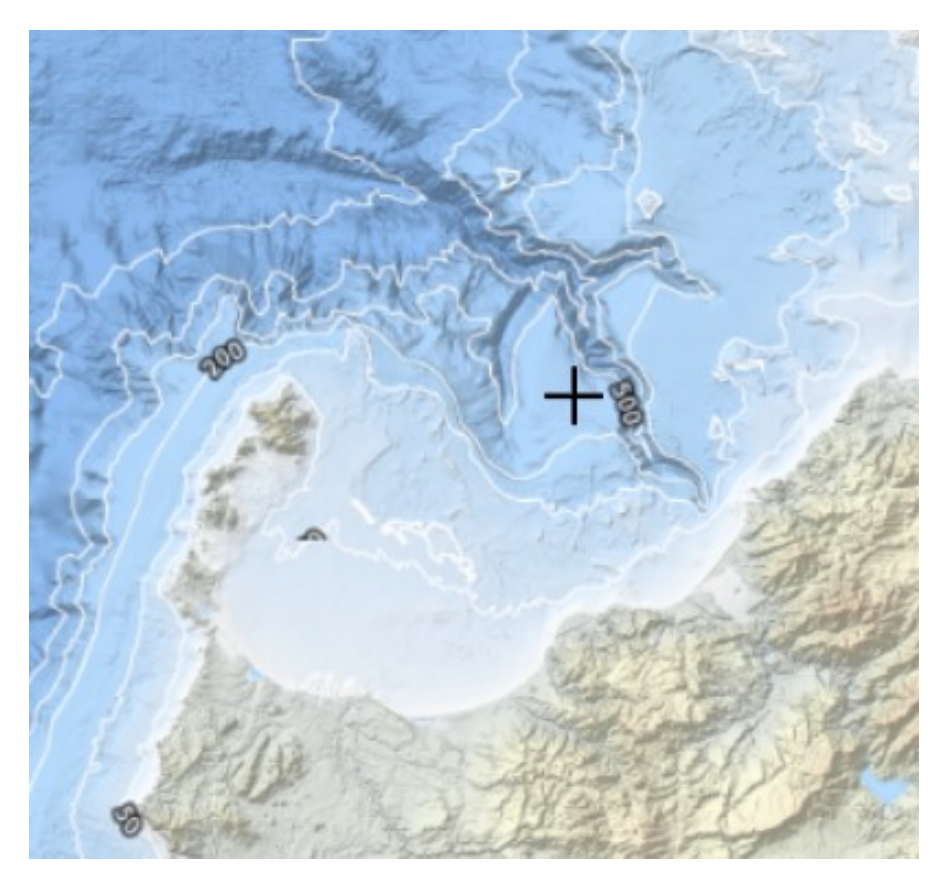


Figure 4.12: Bathymetry contour map. Adapted from [53].

4.2.2 Numerical results

Both algorithms were allowed to run 4 hours and 10 minutes. COBYLA did not reach the stopping tolerance of $1\cdot 10^{-6}$.

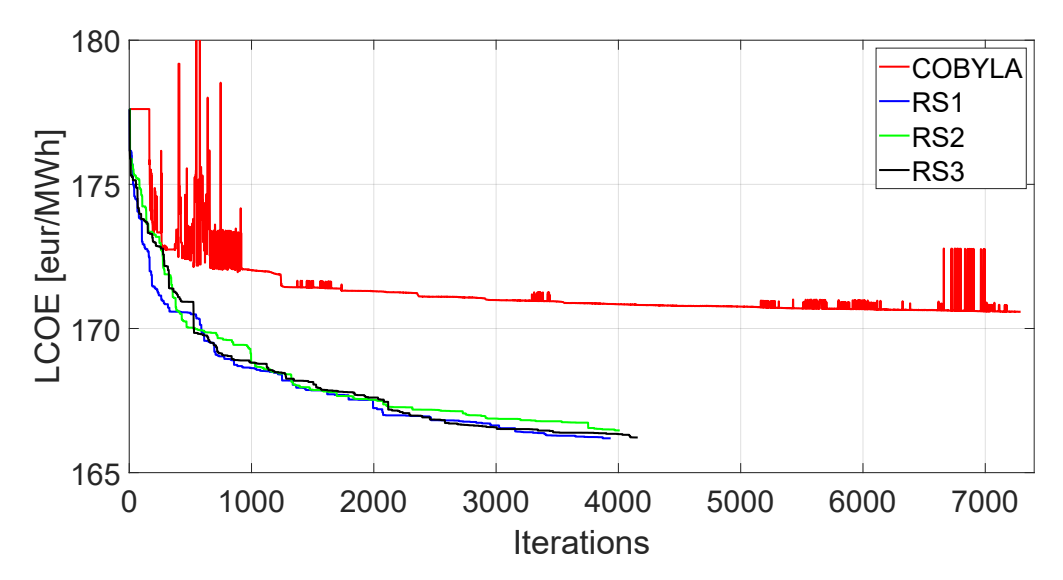


Figure 4.13: LCOE as a function of iterations.

Parameter	COBYLA	RS1	RS2	RS3	
Number of iterations	7287	3936	4011	4158	
Time per iteration [s]	2.06	3.81	3.74	3.61	
LCOE [EUR/MWh]	170.578	166.191	166.446	166.220	
$\mathbf{Delta} [\%]$	3.96	6.43	6.29	6.41	
${\bf IA\ length\ [km]}$	158.1	139.1	138.5	130.3	
Without routing constraint					
LCOE [EUR/MWh]	170.133	165.747	166.036	165.946	
IA length [km]	141.8	122.6	123.3	120.1	

Table 4.3: Simulation results. The initial layout features a LCOE of 177.612 EUR/MWh.

The additional constraint on the cable route increased significantly the computational cost of the optimization process due to the increased complexity of the graph. Compared to the previous case study, the average elapsed time per iteration per turbine was increased by a factor of 5. A simplified boundary may decrease the computational cost, as an high number of vertices in the boundary increases the computations needed to check possible crossings and constraints violations.

RS significantly outperformed COBYLA in all runs for solution quality, although it showed a significantly higher computational time. As in the previous case study, the layout provided by COBYLA resembles the initial layout. RS is able to reduce foundation costs by moving turbines towards lower depth areas. The substation is also moved towards the corner of the excluded area, decreasing the impact of the

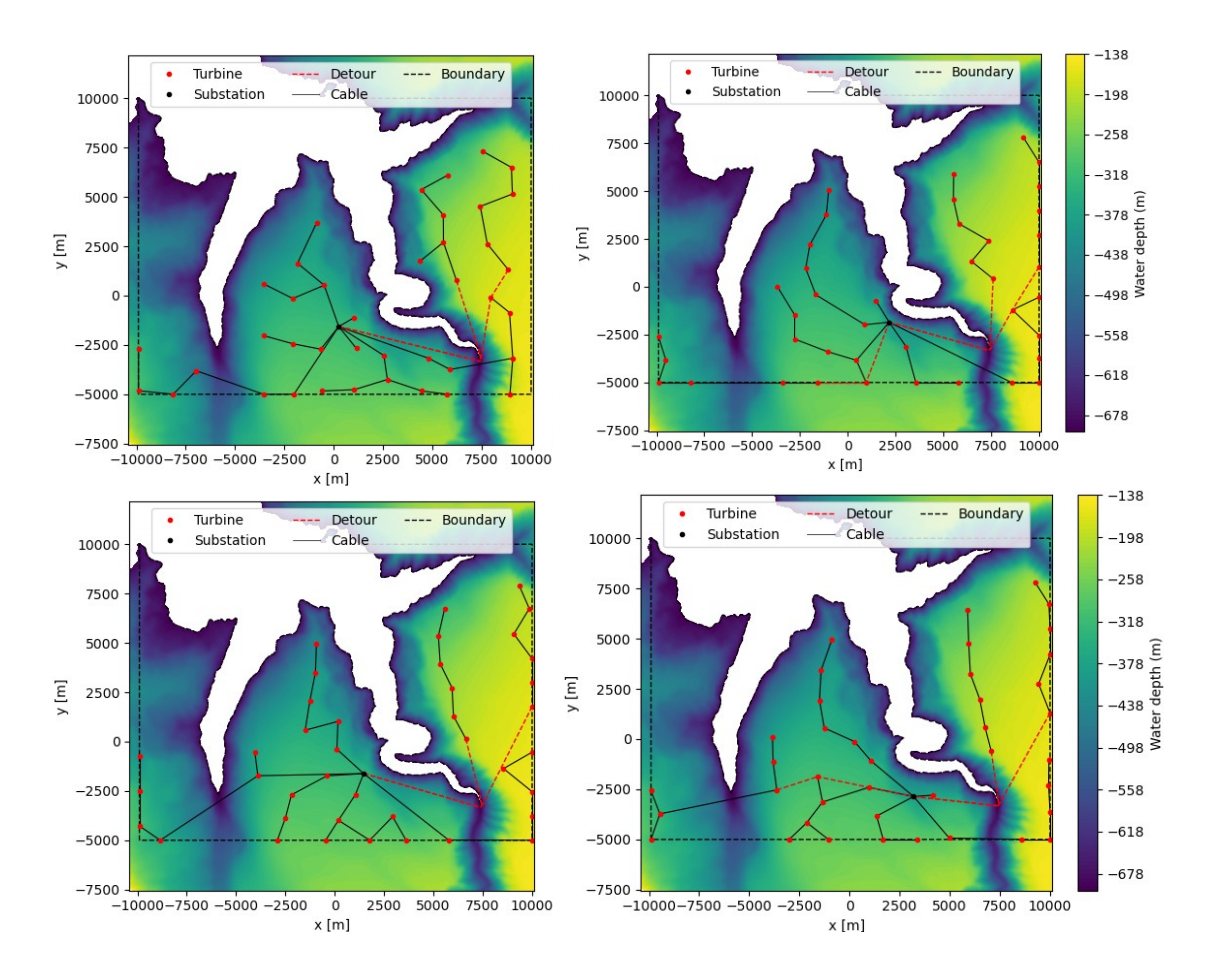


Figure 4.14: Solution provided by COBYLA (top left), RS1 (top right), RS2 (bottom left) and RS3 (bottom right).

cable connection of the easterly turbines on total overall cable length.

The cable routing in the layouts provided by the two optimization algorithms was then solved with the relaxation of the maximum depth constraint. All layouts, except RS3, presented similar reductions in cable length and, as a result, in LCOE. RS3, featuring the shortest overall cable length, however, featured a reduced improvement in the unconstrained conditions.

Chapter 5

Conclusions

The transition to a sustainable and low-carbon energy system relies significantly on harnessing the vast wind resources available in deep waters. In this context, the deployment of floating wind farms in the Mediterranean offers a significant opportunity to unlock the region's generation capacity. In Italy, this process is encouraged by dedicated policy measures designed to support emerging renewable technologies.

Typically, the layout optimization process has been conducted disregarding the Inter Array cable routing and the optimization of the electrical connection was performed once the positioning of turbines was defined. This sequential approach ignores the strong influence that the turbine positioning has on the Inter Array routing. This thesis aims at addressing this gap in the methodology, through the development and application of an integrated optimization framework, that jointly considers both aspects. Notably, the proposed optimization framework also incorporates the optimization of the offshore substation location, representing the main methodological contribution of this thesis.

A comprehensive review of the state of the art in layout optimization informed the selection of appropriate models and algorithms to be adopted. The Jensen top-hat model was chosen to model wake losses, as it has shown good accuracy in AEP estimation and has a low computational cost. The heuristic Random Search algorithm has shown promising results in literature, and its effectiveness was compared to the local search based COBYLA algorithm.

The developed optimization framework integrates two open-source, Python-based tools: OptiWindNet, employed for cable routing optimization under typical constraints such as cable crossing avoidance, and TOPFARM, adopted for the turbine layout and substation position optimization. The co-optimization was implemented using a nested approach, i.e. the routing problem was solved at each iteration of the layout optimization process. The choice of the cable routing optimization algorithm was guided by a consideration on the added computational

burden and the scalability of the time with the number of turbines.

The applicability of the proposed approach was evaluated through two case studies. The first case study, located off the coast of Alghero, was designed to comply with the requirements set by the Italian government to access the support scheme granted by the FER2 decree. Three farm sizes were simulated. In the smallest configuration, consisting of 20 IEA 15 MW turbines, the main driver of optimization consisted in the minimization of the export cable length, while for the other sizes (44 and 66 turbines) the effect was less important. The 44 turbines case showed the lowest LCOE. For this configuration, a sensitivity analysis was conducted, showing a 30 % increased LCOE when the discount rate was raised by 4 %. Among the two algorithms, RS showed significantly improved performances in solution quality in all configurations, although it presented also approximately 20 % increased computational cost.

The second case study was designed to include a more complex bathymetric profile, where a configuration of 40 turbines was analysed. A constraint on the maximum depth of cable routes was imposed, which resulted in approximately a fivefold increase in computational time, highlighting the impact of boundary complexity on computational performance. The RS provided on average 2.5~% lower LCOE with respect to the solution provided by COBYLA, albeit at a higher computational cost.

The adopted optimization framework could benefit from further improvements to overcome its limitations:

- Only one offshore substation is considered. Extending the framework to modelling and optimising farms with more substations would increase the applicability.
- The Inter Array cable configuration can be optimized by modelling the connection with different cable sections, according to the maximum power flow through the segment. This allows to use less expensive cables towards the peripheral area of the farm.
- An estimation of electrical losses could be integrated, to estimate the electrical losses in the wind farm.
- A significant effort in the design of a floating offshore wind farm is dedicated to the sizing of the mooring system, according to seabed substrate and conditions. The framework could be improved by recognising seabed substrate and correctly choosing the appropriate mooring system.

In conclusion, the joint optimization of wind farm layout and cable routing represents a promising methodology to reduce the cost of energy in floating offshore projects. By addressing current limitations and expanding its capabilities, the proposed framework can serve as a valuable tool to support the large-scale deployment of the technology in the Mediterranean Sea.

Appendix A

Cable array approach

To choose between the two approaches, it was chosen to investigate the trade off between added computational cost and solution quality, evaluated as the overall length of the array cables. To estimate computational costs, the most rigorous approach would consist in measuring CPU time, thereby isolating the process from background tasks that might introduce variability. However, this approach was not applied, as such accuracy is beyond the scope of this work. Instead, the elapsed time for each run were measured, with each optimization happening sequentially under same system conditions, in order to reasonably assume that background processes are constant. The tests were performed on a laptop featuring a 8^{th} generation i5 core operating at 1.60 GHz, 8 GB RAM.

Two different layout shapes have been simulated: the first one is the checker configuration, with the substation located on the centre of mass; the second one is the result of smart start pre-optimization (see Figure A.1). The mathematical solver was given, in practice, no maximum solving time.

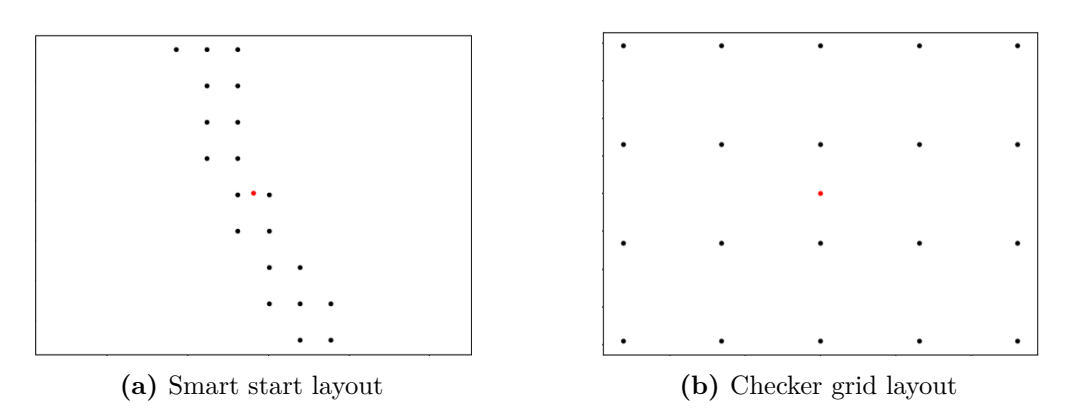


Figure A.1: Example of the two layouts, 20 turbines. The substation is shown in red, while the turbines are shown in black.

The results are shown in Table A.1 and Table A.2.

# turbines	OR. length [km]	OR. time [s]	EW length [km]	\mid EW time [s] \mid
5	2.599	0.02	2.599	0.00
10	5.849	0.03	5.849	0.01
20	12.503	0.08	12.658	0.01
30	19.198	0.13	19.275	0.02
40	25.854	0.22	27.090	0.03
50	33.177	0.38	34.373	0.04

Table A.1: Checker grid configuration results. "OR." refers to the mathematical solver.

# turbines	OR. length [km]	OR. time [s]	EW length [km]	\mid EW time [s] \mid
5	10.264	0.11	10.264	0.01
10	22.376	0.11	22.376	0.01
20	43.779	0.36	45.421	0.10
30	63.451	1.09	63.624	0.02
40	85.644	40.05	87.193	0.09
50	108.804	596.62	112.707	0.05

Table A.2: Smart start configuration results. "OR." refers to the mathematical solver.

From this simple test it is possible to observe that:

- 1. The meta-heuristic always takes less time than the mathematical solver, as expected;
- 2. The mathematical solver computational time grows exponentially with the number of turbines, with a much steeper growth in the smart start configuration (see Table A.2);
- 3. The mathematical solver provides a solution on average 2.4~% better, when different from the heuristic's one.

Even if the mathematical solver was allowed to run without a maximum time; for the 50 turbines case, it took circa 7 seconds to the mathematical solver to reach the optimal solution. However, when given a time limit comparable to the time the heuristic took, no significant improvement was achieved.

Given the adopted framework, using the mathematical solver for cable route optimization is not feasible due to its prohibitive computational time. Moreover,

since the difference in solution quality between the two algorithms is minimal, its impact on the overall optimization process is expected to be negligible.

Appendix B

Cost function

Cost component	Value	Type
Development and consent	179 k€/MW	CAPEX
Wind turbine	1.5 M€/MW	CAPEX
Semi-submergible floater	1.14 M€/MW	CAPEX
Turbine and platform installation	135.5 k€/MW + 0.16 k€/MW/ km_p	CAPEX
Mooring	$C_{mooring} = C_{ref} \cdot f(h)$	CAPEX
Mooring installation	$0.77 \text{ k} \in /\text{MW}/m_d + 0.07 \text{ k} \in /\text{MW}/km_p$	CAPEX
Export cables	$1.8~\mathrm{M} \in /km_s$	CAPEX
Inter Array Cables	$227 k€/km_{cable}$	CAPEX
Cables Accessories	53 k€/MW	CAPEX
Export Cables Installation	55 k€/MW	CAPEX
IA cables installations	190 k€/ km_{cable}	CAPEX
Pull-in, testing and termination	24.8 k€/MW	CAPEX
Offshore substation	179.5 k€/MW	CAPEX
Offshore substation installation	28.8 k€/MW	CAPEX
Onshore substation	97.7 k€/MW	CAPEX
Transport and offshore logistics	13 k€/MW	CAPEX
Contingency and insurance	322.4 k€/MW	CAPEX
Site-clearance fee	$56.4 \ \mathrm{k} \in /km^2$	DECEX
Turbines and platforms	70 % of CAPEX value	DECEX
Cables	10 % of CAPEX value	DECEX
OSS and mooring system	90 % of CAPEX value	DECEX
OPEX	2 % of CAPEX (annually)	OPEX

Table B.1: Full cost function breakdown. The units of distance are differentiated based on the case with subscripts: "d" indicates water depth, "s" indicates distance from shore and "p" indicates distance from port.

The CAPEX is assumed to be a function of the rated power of the farm, water depth,number of turbines, distance from port and distance from shore.

The OPEX is assumed to be a fixed percentage of the CAPEX, set equal to 2 %. This approach is common in literature for its simplicity, however, when taking into account other aspects (e.g. aerodynamic loads on turbine blades [30]) on operational costs a more sophisticated model should be adopted.

Decommissioning costs are assumed to be a percentage of the installation costs per component: 70% for turbines and platforms, 10% for cables, 90% for the offshore substation and mooring system. Furthermore, a site-clearance fee, function of the farm's area is accounted.

Bibliography

- [1] IPCC. Cambiamento climatico 2021: una sintesi per tutti. Tech. rep. IPCC, 2021 (cit. on p. 1).
- [2] Eurostat. Renewable energy statistics Share of renewable energy almost tripled between 2004 and 2023. Accessed: 29 September 2025. European Commission / Eurostat. 2025. URL: https://ec.europa.eu/eurostat/statistics-explained/index.php?title=Renewable_energy_statistics# Share_of_renewable_energy_almost_tripled_between_2004_and_2023 (cit. on p. 1).
- [3] Eurostat. Renewable energy statistics. https://ec.europa.eu/eurostat/st atistics-explained/index.php?title=Renewable_energy_statistics. Data extracted December 2024; accessed 30 September 2025. 2024 (cit. on p. 1).
- [4] RENEWABLE POWER GENERATION COSTS IN 2022. Tech. rep. IRENA, 2022 (cit. on p. 1).
- [5] BVG Associates. Guide to a Floating Offshore Wind Farm. Tech. rep. Report commissioned by Offshore Renewable Energy (ORE) Catapult, The Crown Estate and Crown Estate Scotland. BVG Associates, 2023. URL: https://guidetofloatingoffshorewind.com/ (cit. on pp. 2, 26).
- [6] Riccardo Riva, Jaime Yikon Liew, Mikkel Friis-Møller, Nikolay Krasimirov Dimitrov, Emre Barlas, Pierre-Elouan Réthoré, and Mads Mølgaard Pedersen. Welcome to TOPFARM. URL: https://topfarm.pages.windenergy.dtu.dk/TopFarm2/index.html (cit. on pp. 2, 27).
- [7] Mauricio Souza de Alencar, Amir Arasteh, and Mikkel Friis-Møller. OptiWind-Net: Tool for designing and optimizing the electrical cable network of offshore wind farms. DTU Wind and Energy Systems, Technical University of Denmark, 2025. URL: https://gitlab.windenergy.dtu.dk/TOPFARM/OptiWindNet (cit. on pp. 2, 25).

- [8] G. Mosetti, C. Poloni, and B. Diviacco. «Optimization of wind turbine positioning in large windfarms by means of a genetic algorithm». In: *Journal of Wind Engineering and Industrial Aerodynamics* 51.1 (1994), pp. 105–116. DOI: 10.1016/0167-6105(94)90080-9 (cit. on pp. 3, 4, 6, 12, 24).
- [9] Archer C. L. Vasel-Be-Hagh A. Yan C. Wu S. Pan Y. Brodie J. F. Maguire A. E. «Review and evaluation of wake loss models for wind energy applications.» In: *Applied Energy*, 226, 1187–1207. https://doi.org/10.1016/j.apenergy.2018.05.085 (2018) (cit. on pp. 3, 5, 6, 8, 15, 24).
- [10] Paul Malisani, Tristan Bartement, and Pauline Bozonnet. «Offshore wind farm layout optimization with alignment constraints». In: Wind Energy Science 10 (2025), pp. 1611–1623. DOI: 10.5194/wes-10-1611-2025. URL: https://doi.org/10.5194/wes-10-1611-2025 (cit. on p. 4).
- [11] Ju Feng and Wen Zhong Shen. «Solving the wind farm layout optimization problem using random search algorithm». In: *Renewable Energy* 78 (2015), pp. 182–192. DOI: 10.1016/j.renene.2015.01.005. URL: https://doi.org/10.1016/j.renene.2015.01.005 (cit. on pp. 4, 14).
- [12] Kjersti Solberg Eikrem, Rolf Johan Lorentzen, Ricardo Faria, Andreas Størksen Stordal, and Alexandre Godard. «Offshore wind farm layout optimization using ensemble methods». In: Renewable Energy 216 (2023), p. 119061. DOI: 10.1016/j.renene.2023.119061. URL: https://doi.org/10.1016/j.renene.2023.119061 (cit. on pp. 4, 11).
- [13] Riccardo Travaglini, Francesco Papi, and Alessandro Bianchini. «Floating wind farms in sea basins with moderate wind speeds: a critical assessment of the potential of low-specific-power turbines in reducing the LCoE». In: Renewable and Sustainable Energy Reviews 222 (C 2025). DOI: 10.1016/j.rser.2025.115990 (cit. on pp. 4, 14).
- [14] Davide Cazzaro, David Franz Koza, and David Pisinger. «Combined layout and cable optimization of offshore wind farms». In: *European Journal of Operational Research* 311.1 (2023), pp. 301–315. DOI: 10.1016/j.ejor.2023.04.046 (cit. on pp. 4, 6, 18, 24).
- [15] S. Fragoso Rodrigues, P. Bauer, and P. A. N. Bosman. «Multi-objective optimization of wind farm layouts Complexity, constraint handling and scalability». In: *Renewable and Sustainable Energy Reviews* 65 (2016), pp. 587—609. DOI: 10.1016/j.rser.2016.07.021. URL: https://doi.org/10.1016/j.rser.2016.07.021 (cit. on p. 4).

- [16] Tuhfe Gocmen, Paul van der Laan, Pierre-Elouan Rethore, Alfredo Pena Diaz, Gunner Chr. Larsen, and Soeren Ott. «Wind turbine wake models developed at the Technical University of Denmark: A review». In: Renewable & Sustainable Energy Reviews 60 (2016), pp. 752–769. ISSN: 1364-0321. DOI: 10.1016/j.rser.2016.01.113 (cit. on pp. 5, 8).
- [17] N.O. Jensen. «A note on wind generator interaction». In: (1983) (cit. on pp. 6, 9).
- [18] Accessed on 4/09/2025 (cit. on p. 6).
- [19] Herbert-Acero J. Probst O. Réthoré P. Larsen G. Castillo-Villar K. «A review of methodological approaches for the design and optimization of wind farms.» In: *Energies*, 7(11), 6930–7016. (2014) (cit. on pp. 6, 24).
- [20] S. Frandsen, R.J. Barthelmie, S. Pryor, O. Rathmann, S. Larsen, J. Højstrup, and M. Thøgersen. «Analytical modelling of wind speed deficit in large offshore wind farms». In: *Wind Energy* 9 (2006), pp. 39–53. DOI: 10.1002/we.189 (cit. on p. 7).
- [21] Omid Rahbari, Majid Vafaeipour, Farivar Fazelpour, Michel Feidt, and Marc A. Rosen. «Towards realistic designs of wind farm layouts: Application of a novel placement selector approach». In: *Energy Conversion and Management* 81 (2014), pp. 242–254. DOI: 10.1016/j.enconman.2014.02.019 (cit. on p. 8).
- [22] Gunner C. Larsen. A Simple Wake Calculation Procedure. Risø-M; No. 2760. Risø National Laboratory, Copenhagen, Denmark, 1988 (cit. on p. 8).
- [23] Gunner Chr. Larsen. A simple stationary semi-analytical wake model. Tech. rep. 1713(EN). Risø National Laboratory for Sustainable Energy, Technical University of Denmark, 2009 (cit. on p. 8).
- [24] Byeongho Hwang, Hyunkee Kim, and Soogab Lee. «Wind farm layout optimization using multidisciplinary model». In: *Journal of Mechanical Science and Technology* 32.6 (2018), pp. 2919–2924. DOI: 10.1007/s12206-018-0548-3 (cit. on p. 9).
- [25] Bastankhah M. and Porté-Agel F. «A new analytical model for wind-turbine wakes». In: *Renewable Energy* (2014) (cit. on pp. 9, 10).
- [26] *Optimization*. In: ed. by Oxford University Press. Accessed on 2 September 2025. 2024 (cit. on p. 11).
- [27] Rabia Shakoor, Mohammad Yusri Hassan, Abdur Raheem, and Yuan-Kang Wu. «Wake effect modeling: A review of wind farm layout optimization using Jensen's model». In: *Renewable and Sustainable Energy Reviews* 58 (2016), pp. 1048–1059. DOI: 10.1016/j.rser.2015.12.229 (cit. on p. 12).

- [28] Siyu Tao, Qingshan Xu, Andrés Feijóo, Gang Zheng, and Jiemin Zhou. «Nonuniform wind farm layout optimization: A state-of-the-art review». In: *Energy* 209 (2020), p. 118339. DOI: 10.1016/j.energy.2020.118339 (cit. on p. 13).
- [29] Souma Chowdhury, Jie Zhang, Achille Messac, and Luciano Castillo. «Unrestricted Wind Farm Layout Optimization (UWFLO): Investigating key factors influencing the maximum power generation». In: *Renewable Energy* 38.1 (Jan. 2012), pp. 16–30. DOI: 10.1016/j.renene.2011.06.033 (cit. on pp. 13, 24).
- [30] M.J.D. Powell. «A Direct Search Optimization Method That Models the Objective and Constraint Functions by Linear Interpolation». In: Advances in Optimization and Numerical Analysis (1994) (cit. on pp. 13, 52).
- [31] Riccardo Riva, Jaime Yikon Liew, Mikkel Friis-Møller, Nikolay Dimitrov, Emre Barlas, Pierre-Elouan Réthoré, and Arvydas Beržonskis. «Wind farm layout optimization with load constraints using surrogate modelling». In: *Journal of Physics: Conference Series*. IOP Publishing, 2020. DOI: 10.1088/1742-6596/1618/4/042035 (cit. on p. 14).
- [32] Ju Feng and Wen Zhong Shen. «Optimization of Wind Farm Layout: A Refinement Method by Random Search». In: Proceedings of the 2013 International Conference on Aerodynamics of Offshore Wind Energy Systems and Wakes (ICOWES2013). Technical University of Denmark, 2013. URL: https://orbit.dtu.dk/en/publications/optimization-of-wind-farm-layout-a-refinement-method-by-random-se (cit. on p. 14).
- [33] Justin S. Gray, John T. Hwang, Joaquim R. R. A. Martins, Kenneth T. Moore, and Bret A. Naylor. «OpenMDAO: An open-source framework for multidisciplinary design, analysis, and optimization». In: Structural and Multidisciplinary Optimization 59.4 (2019), pp. 1075–1104. DOI: 10.1007/s00158-019-02211-z (cit. on pp. 17, 27).
- [34] Mads M. Pedersen et al. PyWake 2.5.0: An open-source wind farm simulation tool. DTU Wind, Technical University of Denmark, 2023. URL: https://gitlab.windenergy.dtu.dk/TOPFARM/PyWake (cit. on pp. 17, 23, 24).
- [35] NREL. «FLORIS. Version 4.2.1». In: GitHub repository (2024). URL: https://github.com/NREL/floris (cit. on p. 17).
- [36] Rafael Mudafort and National Renewable Energy Laboratory. WETO Software Stack. Accessed: 2025-09-26. 2024 (cit. on p. 17).
- [37] Vind AI. Vind AI. Accessed: 2025-09-25. 2025 (cit. on p. 17).
- [38] EMD International A/S. windPRO Modules. Accessed: 2025-09-25. 2025 (cit. on p. 18).

- [39] UL Renewables. OpenWind Wind Farm Modeling & Layout Design Software. https://ul-renewables.com/openwind/. Accessed: 2025-09-26. 2025 (cit. on p. 18).
- [40] Tyler Stehly, Patrick Duffy, and Daniel Mulas Hernando. Cost of Wind Energy Review: 2024 Edition. Tech. rep. NREL/PR-5000-91775. Golden, CO (United States): National Renewable Energy Laboratory (NREL), 2024. URL: https://www.nrel.gov/docs/fy25osti/91775.pdf (cit. on p. 22).
- [41] Kun Xu, Kjell Larsen, Yanlin Shao, Hyun-Cheol Kim, Jinbao Wang, and Zhi Zong. «Design and comparative analysis of alternative mooring systems for floating wind turbines in shallow water with emphasis on ultimate limit state design». In: *Ocean Engineering* 223 (2021), p. 108653. DOI: 10.1016/j.oceaneng.2020.108653 (cit. on p. 23).
- [42] Alessandro Sebastiani, Alfredo Peña, Niels Troldborg, and Alexander Meyer Forsting. «Evaluation of the global-blockage effect on power performance through simulations and measurements». In: Wind Energy Science 7.2 (2022). Accessed: 2025-09-26, pp. 875-886. DOI: 10.5194/wes-7-875-2022. URL: https://wes.copernicus.org/articles/7/875/2022/ (cit. on p. 25).
- [43] Leszek Resner and Sandra Paszkiewicz. «Radial Water Barrier in Submarine Cables, Current Solutions and Innovative Development Directions». In: *Energies* 14.10 (2021), p. 2761. DOI: 10.3390/en14102761 (cit. on p. 25).
- [44] Laurent Perron and Frédéric Didier. *CP-SAT*. Version v9.10. Google, May 7, 2024. URL: https://developers.google.com/optimization/cp/cp_solver/(cit. on p. 25).
- [45] Manuel U. T. Rentschler, Frank Adam, Paulo Chainho, Kilian Krügel, and Pedro C. Vicente. «Parametric study of dynamic inter-array cable systems for floating offshore wind turbines». In: *Marine Systems & Ocean Technology* 15.1 (2020), pp. 16–25. DOI: 10.1007/s40868-020-00071-7. URL: https://link.springer.com/article/10.1007/s40868-020-00071-7 (cit. on p. 27).
- [46] SSE Renewables. Second HVDC offshore substation platform installed at Dogger Bank Wind Farm. 2024. URL: https://www.sserenewables.com/news-and-views/2024/04/second-hvdc-offshore-substation-platform-installed-at-dogger-bank-wind-farm/?utm_source=chatgpt.com (visited on 09/24/2025) (cit. on p. 27).
- [47] Mpower s.r.l. Progetto di una centrale eolica offshore galleggiante nel mare di Sardegna denominata "Sardinia North-West" e delle relative opere di connessione alla rete elettrica nazionale. Studio Preliminare Ambientale. Relazione Tecnica Generale R.01. Art. 21, D.Lgs. n. 152/2006 Definizione dei contenuti

- SIA (Scoping). Italia: AvenHexicon S.r.l., Mpower S.r.l., 2022 (cit. on pp. 27, 30).
- [48] Maria Sarcos, Julian Quick, Andrea N. Hahmann, Nicolas G. Alonso-De-Linaje, Neil Davis, and Mikkel FriisMøller. «Need For Speed: Fast Wind Farm Optimization». In: *The Science of Making Torque from Wind (TORQUE 2024), Journal of Physics: Conference Series.* Vol. 2767. IOP Publishing, 2024. DOI: 10.1088/1742-6596/2767/9/092088 (cit. on p. 28).
- [49] Wikipedia contributors. Aree naturali protette della Sardegna. https://it.wikipedia.org/wiki/Aree_naturali_protette_della_Sardegna. Accessed: 2025-10-02. 2025 (cit. on p. 30).
- [50] Ministero dell'Ambiente e della Sicurezza Energetica and della Sovranità Alimentare e delle Foreste Ministero dell'Agricoltura. Decreto FER 2 19-06-2024. https://www.gse.it/documenti_site/Documenti%20GSE/Servizi%20per%20te/FER2/Normativa/DM%20FER%202%2019-06-2024. pdf. Gazzetta Ufficiale / Official decree, accessed: 2025-09-16. 2024 (cit. on pp. 30, 38).
- [51] S. Schimanke et al. CERRA sub-daily regional reanalysis data for Europe on height levels from 1984 to present. Copernicus Climate Change Service (C3S) Climate Data Store (CDS). DOI: 10.24381/cds.38b394e6, Accessed on 23-05-2025. 2021 (cit. on pp. 30, 31).
- [52] Stylianos Hadjipetrou and Phaedon Kyriakidis. «High-Resolution Wind Speed Estimates for the Eastern Mediterranean Basin: A Statistical Comparison Against Coastal Meteorological Observations». In: Wind 4.4 (2024), pp. 311–341. DOI: 10.3390/wind4040016. URL: https://doi.org/10.3390/wind4040016 (cit. on p. 31).
- [53] Directorate-General for Maritime Affairs European Commission and Fisheries. What is EMODnet? https://emodnet.ec.europa.eu/en/about_emodnet. Accessed: 2025-09-16. 2025 (cit. on pp. 31, 33, 42).
- [54] URL: https://cdi-bathymetry.seadatanet.org/report/edmo/252/cnr-iamc-24 (cit. on p. 32).
- [55] URL: https://cdi-bathymetry.seadatanet.org/report/edmo/252/cnr-iamc-29 (cit. on p. 32).
- [56] URL: https://cdi-bathymetry.seadatanet.org/report/edmo/252/cnr-iamc-27 (cit. on p. 32).

- [57] Ørsted. Offshore Wind at a Crossroads: Reviving the Industry to Secure Europe's Energy Future. Tech. rep. whitepaper. Accessed: 2025-09-29. Ørsted, 2025. URL: https://cdn.orsted.com/-/media/www/docs/corp/com/about-us/whitepaper/offshore-wind-at-a-crossroads.pdf?hash=29AA7DCB2B08881DD58C8937047439A3&rev=54cfc4b44cfb4a5a861d6724e1753342&utm_source=chatgpt.com (cit. on p. 38).
- [58] Vestas. V236-15.0 MWTM. https://www.vestas.com/en/energy-solutions/offshore-wind-turbines/V236-15MW. Accessed: 2025-09-30. 2025 (cit. on p. 39).
- [59] Adrijana Buljan. «Five 20-Year-Old Danish Offshore Wind Farms Seeking Lifetime Extension». In: Offshore WIND.biz (2023). Accessed: 2025-09-30. URL: https://www.offshorewind.biz/2023/12/11/five-20-year-old-danish-offshore-wind-farms-seeking-lifetime-extension/ (cit. on p. 39).
- [60] URL: https://cdi-bathymetry.seadatanet.org/report/edmo/1338/iim 9034-3 (cit. on p. 41).